REPORT DOCUMENTATION PAGE

1a Report Security Classification: Unclassified		1b Restrictive Markings		
2a Security Classification Authority		3 Distribution/Availability of Report		
2b Declassification/Downgrading Schedule		Approved for public release; distribution is unlimited.		
4 Performing Organization Report Number(s)		5 Monitoring Organization Report Number(s)		
6a Name of Performing Organization Naval Postgraduate School	6b Office Symbol *(if applicable)* *52	7a Name of Monitoring Organization Naval Postgraduate School		
6c Address *(city, state, and ZIP code)* Monterey CA 93943-5000		7b Address *(city, state, and ZIP code)* Monterey CA 93943-5000		
8a Name of Funding/Sponsoring Organization	6b Office Symbol *(if applicable)*	9 Procurement Instrument Identification Number		
Address *(city, state, and ZIP code)*		10 Source of Funding Numbers		
		Program Element No	Project No	Task No	Work Unit Accession N

11 Title *(include security classification)* COMPUTATIONAL AND EXPERIMENTAL INVESTIGATION OF THE AERODYNAMIC CHARACTERISTICS OF A WINDSURFING SAIL SECTION

12 Personal Author(s) Matthew Avila

13a Type of Report	13b Time Covered	14 Date of Report *(year, month, day)*	15 Page Count
Engineer's Thesis	From To	December 1992	75

16 Supplementary Notation The views expressed in this thesis are those of the author and do not reflect the official policy or position of the Department of Defense or the U.S. Government.

17 Cosati Codes			18 Subject Terms *(continue on reverse if necessary and identify by block number)*
Field	Group	Subgroup	Aerodynamics, Computational Fluid Dynamics, Sailing

19 Abstract *(continue on reverse if necessary and identify by block number)*

In this thesis results of a computational and experimental investigation of the aerodynamic characteristics of a sail section used in windsurfing sails are presented. State-of-the-art computational methods (panel, direct boundary layer, viscous-inviscid interaction, Euler, and steady/unsteady Navier-Stokes) were used to predict the aerodynamic loading and stall characteristics. These predictions were found to be in satisfactory agreement with tuft and smoke flow visualization experiments carried out in the Naval Postgraduate School low speed wind tunnel at a Reynolds number of 800,000. Further, all computational work was completed on the Silicon Graphics Indigo workstation to demonstrate that only modest computer facilities will be necessary for these methods to migrate to the field of sail design.

20 Distribution/Availability of Abstract	21 Abstract Security Classification	
__ unclassified/unlimited __ same as report __ DTIC users	Unclassified	
22a Name of Responsible Individual Professor M. F. Platzer	22b Telephone *(include Area Code)* 656-2058	22c Office Symbol AA/Pl

D FORM 1473,84 MAR 83 APR edition may be used until exhausted security classification of this pa

All other editions are obsolete Unclassifie

T260188

Approved for public release; distribution is unlimited.

Computational and Experimental Investigation of the Aerodynamic Characteristics of a Windsurfing Sail Section

by

Matthew R. Avila
Lieutenant, United States Navy
B.S. United States Naval Academy, 1984

Submitted in partial fulfillment
of the degree requirements for the degree of

AERONAUTICAL AND ASTRONAUTICAL ENGINEER

from the

NAVAL POSTGRADUATE SCHOOL

December 1992

ABSTRACT

In this thesis results of a computational and experimental investigation of the aerodynamic characteristics of a sail section used in windsurfing sails are presented. State-of-the-art computational methods (panel, direct boundary layer, viscous-inviscid interaction, Euler, and steady/unsteady Navier-Stokes) were used to predict the aerodynamic loading and stall characteristics. These predictions were found to be in satisfactory agreement with tuft and smoke flow visualization experiments carried out in the Naval Postgraduate School low speed wind tunnel at a Reynolds number of 800,000. Further, all computational work was completed on the Silicon Graphics Indigo workstation to demonstrate that only modest computer facilities will be necessary for these methods to migrate to the field of sail design.

c.1

TABLE OF CONTENTS

I. INTRODUCTION 1

II. COMPUTATIONAL APPROACH 6

A. GENERAL 6

B. SAIL SHAPE GENERATION TECHNIQUE 6

C. PANEL CODE 11

D. BOUNDARY LAYER CODES 14

E. EULER AND NAVIER-STOKES METHOD 15

F. GRID GENERATION 16

III. EXPERIMENTAL APPROACH 22

A. BACKGROUND 22

B. WIND TUNNEL EXPERIMENTAL EQUIPMENT 22

C. WIND TUNNEL MODEL CONSTRUCTION 26

D. FLOW VISULIZATION 27

IV. RESULTS 29

A. COMPARISON OF THE COMPUTED PRESSURE DISTRIBUTIONS . 29

B. VELOCITY VECTOR PLOTS 35

C. UNSTEADY MOTION 38

V. CONCLUSIONS 46

LIST OF REFERENCES 46

APPENDIX A: 49

INITIAL DISTRIBUTION LIST 68

ACKNOWLEDGEMENTS

I would like to recognize a few of the many people who have contributed to this effort. First, I would like to extend my sincere thanks to Professor Platzer, my thesis advisor, for allowing me the opportunity to explore the subject sailing aerodynamics in addition to his assistance and insight to the problem. Next I wish to recognize my thesis co-advisors Professor Ekaterinaris for his assistance in the Navier-Stokes portion of the computational study and Professor Hebbar for his help in setting up the experimental portion of the thesis.

Similarly, I would like to thank Dr. Tuncer and Prof. Hobson for their assistance on various CFD aspects I had difficulty with and to Tony Cricelli for assisting me in the process of learning computer systems available in the CFD laboratory.

Finally, I would like to thank Trevor Bayless for donating his time and materials in building the wind tunnel model and for sharing his opinions on the status of sail design.

I. INTRODUCTION

The field of computational fluid dynamics (CFD) has come of age over the past several years. Rapid advances in high speed digital computers, their subsequent lower cost and the maturation of CFD codes suggest that CFD methods should spread to areas beyond the aerospace industry in the near future. The discipline of competitive sailing is a promising area that could benefit from the use of CFD techniques. Some have suggested that such applications would be trivial. However, experience shows that sailing is a fiercely competitive sport ranging from amateur levels to Olympic, professional and the America's Cup levels. In practical terms, the bottom line has always been performance, which directly relates to the incorporation of technology into the design process. The aim of this research will be to demonstrate that CFD techniques may be readily adapted to the field of sail design.

From an engineering standpoint, sailing craft are challenging due to the interaction or coupling of two different fluid media, the water's surface and the atmosphere. Additionally, the two media are subject to separate noise or turbulence in the form of waves, wind gradient and gusts. The objective of this thesis will be to apply CFD techniques to the analysis of the above water portion of the problem and to provide some experimental verification. The scope of the analysis will be limited to a two-dimensional approach. A full three-dimensional analysis would have been optimum, but the complexity of the problem and computing power required would have become excessive.

There are numerous rig and sail configurations which ought to be analyzed. Planing hull sailing craft, in general, are more challenging because they are capable of higher speeds than displacement hull yachts. Planing hull craft, moreover, experience a pronounced rise in drag prior to transitioning from a displacement hull mode to a planing hull.

For this study a sailboard or windsurfer rig was selected over other rig and sail combinations for several reasons. The primary reason for the selection of this rig and sail combination is the rig's simplicity, Figure 1.1. Its shape is approximate to a simple wing or foil shape of moderate aspect ratio and is favorable when compared to a sloop or other multi-sail configuration. The acceleration through the above mentioned planing transition is of high interest for study. This acceleration or quick planing ability is of paramount importance to the competitive sailor on any planing hull dingy or sailboard. To accelerate quickly the sailor in effect must generate large lift coefficients from the sail. This is achieved through a large sheeting angle (high angle of attack) in combination with the highly cambered shape built into the sail section and in the case of the board sailor through the dynamic sheeting or pumping of the sail. The effects of pumping are well known to all competitive sailors. However, this sailing technique is strictly prohibited in all classes except some types of boardsailing. The pumping method utilized is a refined art to many board sailors to the degree that sail designers and competitors note this quality in sails.

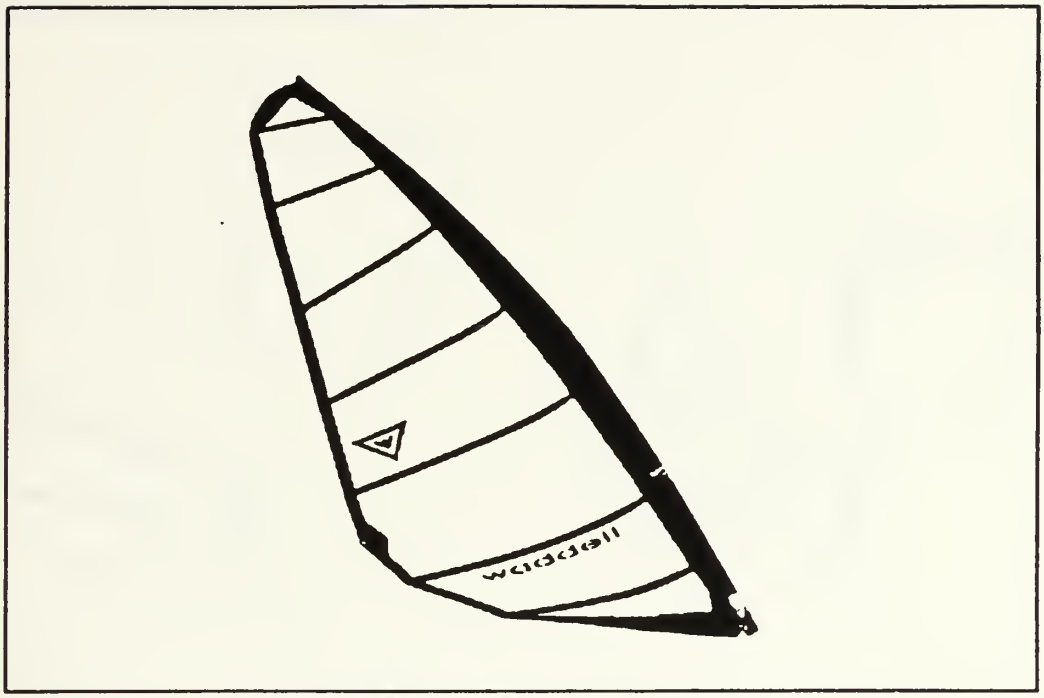

Figure 1.1 WindSurfing Sail

The second regime in which the sail performance is critical occurs after the craft has fully accelerated on a plane. As a craft accelerates the apparent wind shifts forward from the sailor's frame of reference while the true wind velocity remains constant, Figure 1.2. While sailing with the apparent wind far forward the sail is trimmed at or near the maximum lift to drag ratio. The maximum lift to drag ratio in fact limits how close to the wind a vessel may sail or the minimum apparent wind angle that may be sailed.

The technical challenge for analysis in this regime of aerodynamics lies with the low Reynolds number (Re) below one million. The bulk of data to date for airfoil sections is for Reynolds numbers above one million. CFD work has been done at

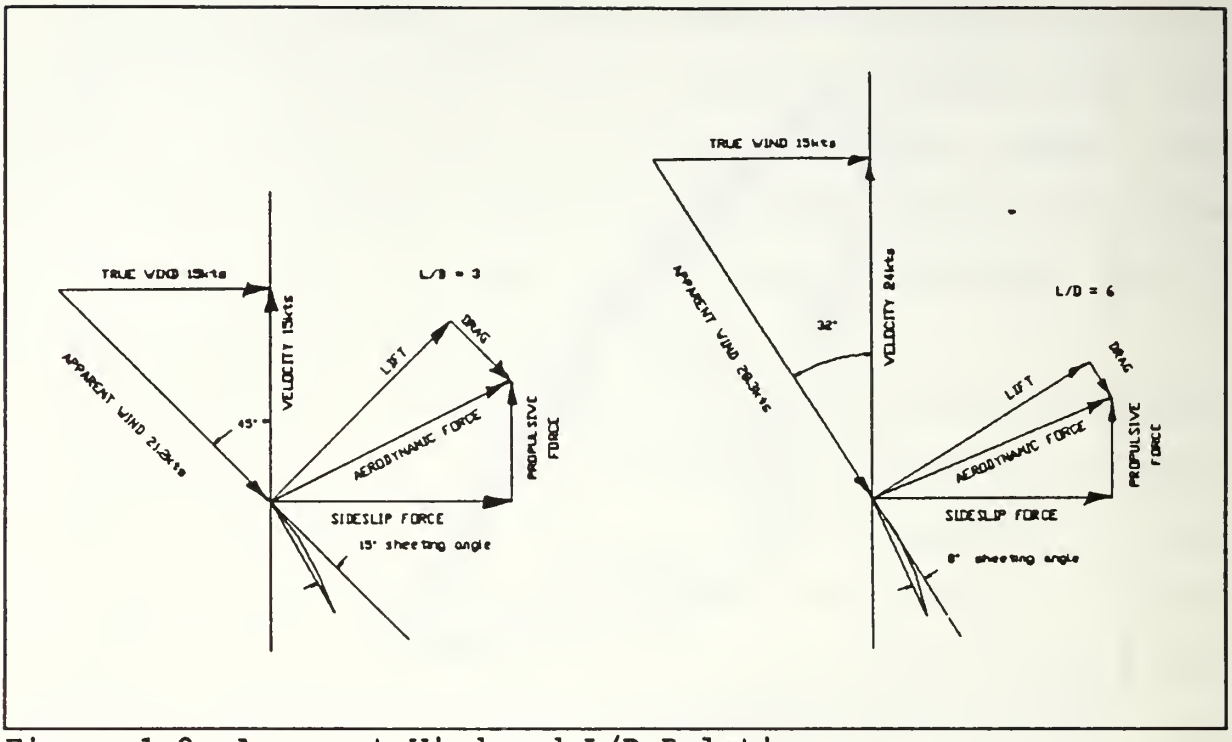

Figure 1.2 Apparent Wind and L/D Relation

Reynolds number below one million, but the work has been frequently restricted to internal flows in turbines or ducts or to research for high altitude aircraft where the Mach numbers are significant. The low Reynolds number implies that the viscous forces will be large and require thorough investigation. This will require the use of viscid codes in addition to simplified inviscid codes to understand the nature of the flow field. On the positive side, the problem is somewhat simplified in that it is entirely incompressible. Physical limitations on the materials used and the method in which sails are constructed produce irregularities and rough surfaces near the leading edge of the sections. These imperfections, while not desirable, allow for the assumption that the flow is fully turbulent. This assumption precludes the

requirement for and validation of a boundary layer transition model.

II. COMPUTATIONAL APPROACH

A. GENERAL

Computational fluid dynamics has been largely restricted to well funded aerospace research and development groups due to the need for access to computers with sufficient power, speed and graphics capability. However, recent advances in computer hardware have eliminated the requirement for access to a super computer to conduct CFD studies. To demonstrate that CFD technology is mature enough to migrate to the field of sail design, the computational work for this study was conducted on Silicon Graphics Indigo and Iris workstations utilizing Fortran codes and Plot 3D for graphics presentation. This generation of workstations have largely redefined the conventional boundaries between workstations, mainframes and mini-supercomputer systems. The level of computing below the Unix workstation has also progressed rapidly with the latest generation of personal computers (PC) built around the Intel 80486 processors. These computers probably have sufficient memory and speed for this application. However, at this time they are limited by a lack of software which has been widely available for the Unix operating system. It may be possible in the near future that new operating systems for the PC will include the necessary software features. The Unix based workstation, while a step above the PC is still well, within the resources of the sail design and manufacture business.

B. SAIL SHAPE GENERATION TECHNIQUE

To commence the study of an airfoil the first requirement encountered is a precise definition of the airfoil section. To proceed with the analysis of a sail section it is necessary to develop a systematic method of describing sail shapes with a similar high degree of precision.

Sail design has never been an exact science. However, sail designers and sailors have always given attention to the same parameters that we see in airfoil design. The maximum camber and

its location aft of the leading edge are the two primary parameters used to describe a sail's shape (the camber of a sail is most commonly referred to as the 'draft' by the sailing community). Several additional parameters are used to further describe the windsurfing sail section. The mast (vertical load bearing spar) has a cylindrical section internal to the leading edge or luff portion of the sail. The mast radius is directly analogous to the leading edge radius used in the definition of many airfoil sections. From the mast section aft two flat panels are used to fair the mast cross section to the thin segment of the section that compose the majority of the sail. The length of this faring has been defined as the luff pocket length.

A fortran code, 'shape.f' Appendix A, was developed to precisely define a sail section based on the geometric parameters mentioned above. Two models for the camber line generation have been included in the program. For a large number of sails the camber line can be approximated by a circular arc aft of the maximum camber location and with a second order polynomial forward. This model is the first camber option for sail generation which requires the following input arguments:

mast radius (2.0% nominal value)
luff pocket length
thickness
maximum camber or draft
maximum camber location

To describe a more unique section with flat segments or reflexed areas a higher order polynomial fit has been included as the second option for camber generation. For this routine the camber line is defined by points through which a Lagrange polynomial is fitted. The first three input parameters for this option remain the same but in place of the maximum camber and location the user enters **n** number of **x,y** coordinates to define the camber shape.

'Shape.f' builds the section from the common trailing edge point working forward. The generation routine uses the selected

camber model to describe the sail camber shape aft of the luff dimension with an increment to add the prescribed thickness. From the luff dimension forward a straight line is placed tangent tHxthe mast radius to describe the shape. Seventy panels top and bottom from the trailing edge point are used to this point and a final ten panels are used to depict the mast radius. The 151 **x,y** coordinates that form the basic geometry of the section are written into a file 'shape.out.'

A final segment of 'shape.f' adds thirty wake points extended tangent to the trailing edge for grid generation use. The length between the wake points begins with the same initial dx distance with each subsequent length expanded by a factor of 1.1. This second set of data points including the wake points is written to 'hypgen.out' for subsequent grid generation use.

The primary shape used for the CFD evaluation and tunnel testing is depicted in Figure 2.1. This section shape was typical of the first fully battened sails appearing in the mid-1980's. The shapes used at that time were generally highly cambered with the maximum camber well forward of the mid-chord point. The shape depicted is irregular, in particular the forward segment, when compared to a conventional airfoil. Obviously, a better shape from an aerodynamic perspective would be desirable but physical limitations with the mast, materials and manufacture prevent the building of 'ideal' sections.

Sail shapes have slowly evolved through a process of trial and error into shapes similar to that in Figure 2.2. The current shapes have less camber with the maximum camber point closer to the mid-cord. The shapes shown in Figures 2.1/2 were both generated using the circular arc and second order polynomial method. The 'shape.out' files containing the **x,y** stations for the two sections are contained in Appendix A.

Current interest among sail makers has been to make the aft sections increasingly flat. The shapes may promise to perform better. However, the flat areas are difficult to build into the sail and are prone to flutter. An advanced shape similar to the ones

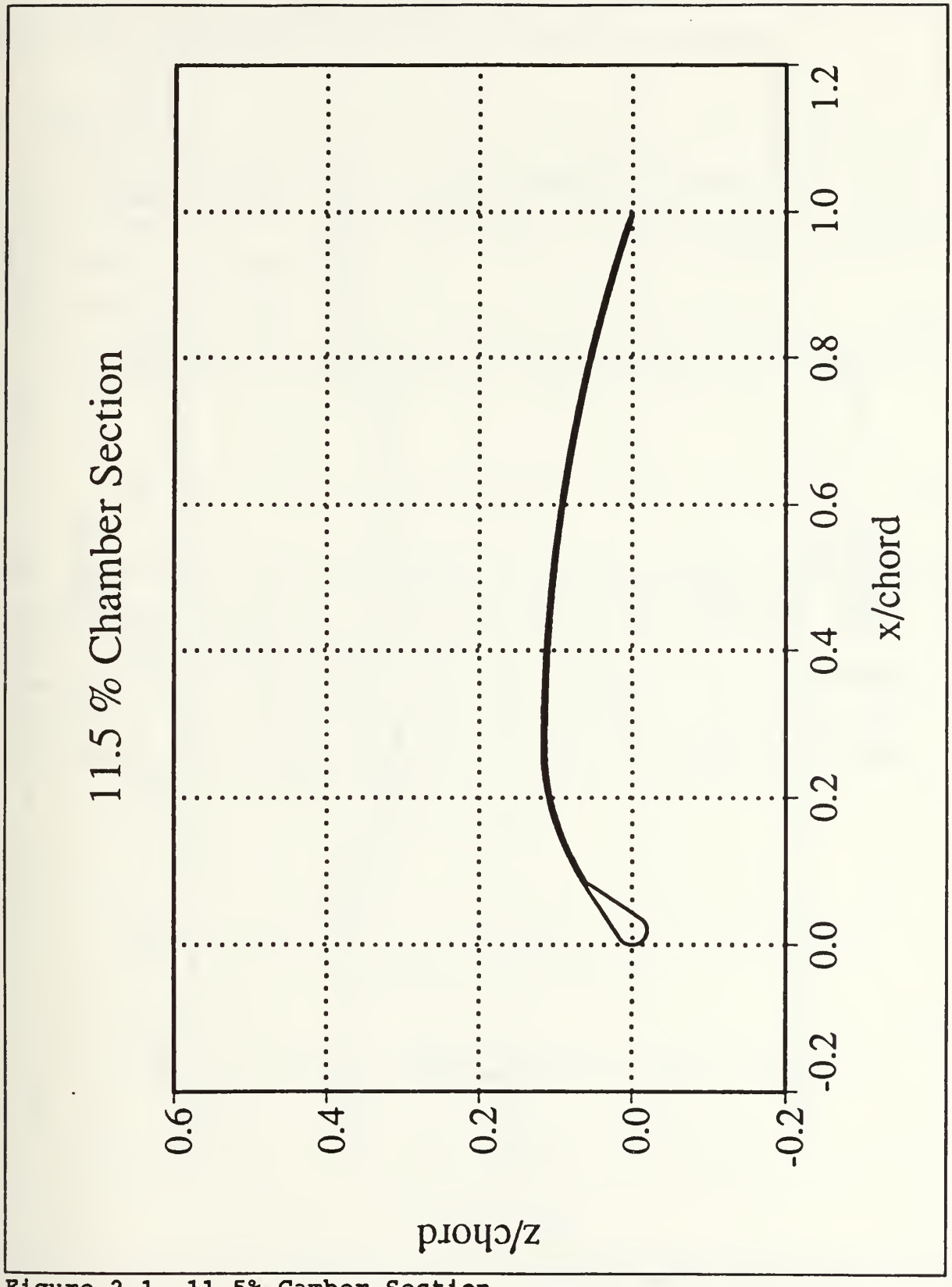

Figure 2.1 11.5% Camber Section

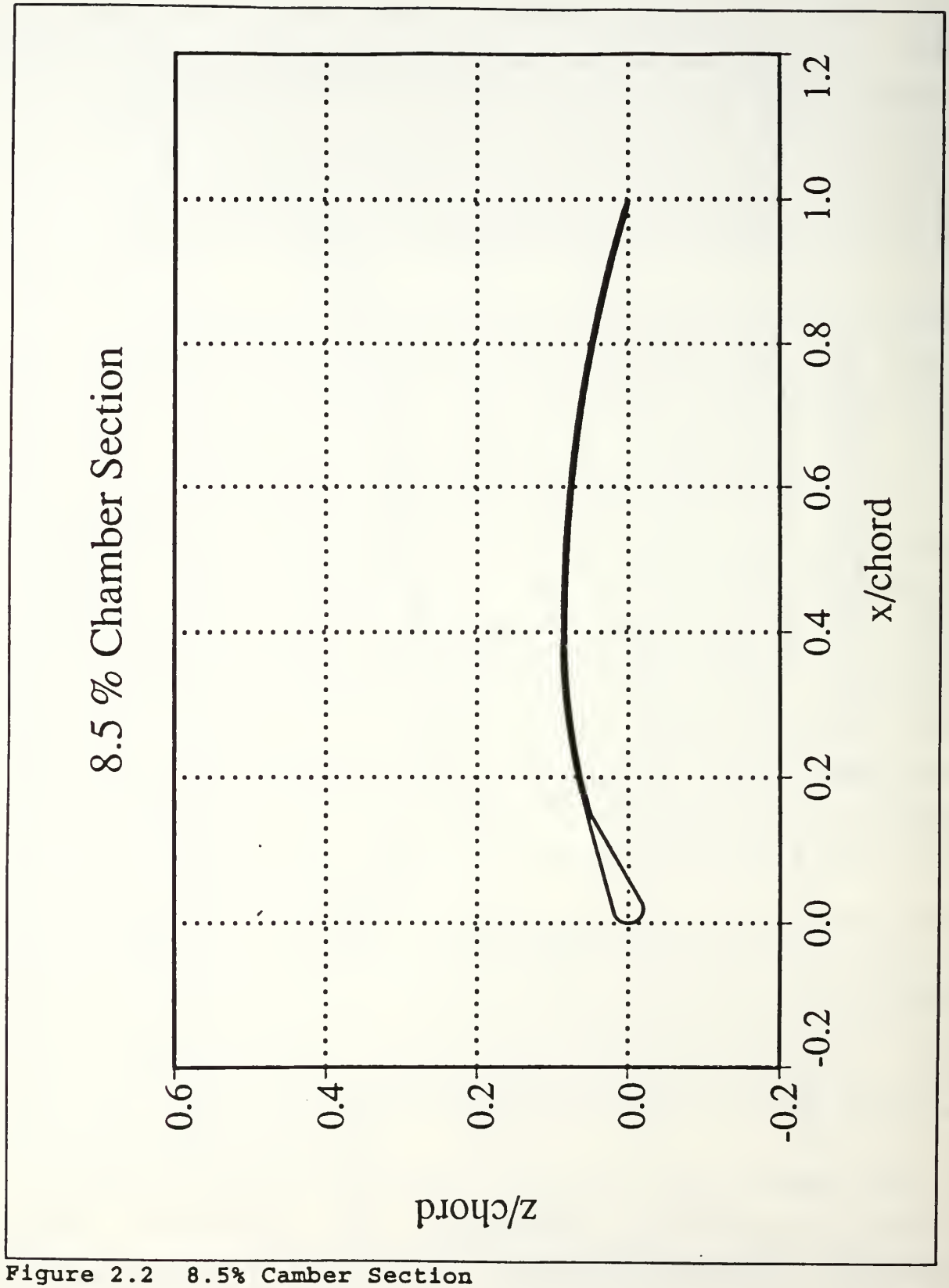

Figure 2.2 8.5% Camber Section

currently being tested was derived utilizing the Lagrange polynomial generation method and is shown in Figure 2.3.

C. PANEL CODE

Panel codes represent an introductory means to model the flow field around a body. They are the simplest and easiest method to explore the flow field for the subject of this thesis. Of note, this family of codes can easily run solutions and be plotted on a modest personal computer.

To explain the panel method we first examine Laplace's equation governing incompressible, irrotational, and invisid fluid flow:

$$\Phi_{xx}+\Phi_{yy}=0 \tag{2.1}$$

This expression is a homogeneous linear second order partial differential equation. The linearity of the equation allows the use of the superposition principle to describe the flow field with elementary flow elements. For the case of a two dimensional airfoil in a uniform flow the system may be expressed as a combination of uniform, source and vortex potential elements:

$$\Phi=\Phi_{\infty}+\Phi_{s}+\Phi_{v} \tag{2.2}$$

where

$$\Phi_{\infty}=V_{\infty}(x\cos\alpha+y\sin\alpha)$$

$$\Phi_{s}=\frac{\Delta}{2\pi}\ln r \tag{2.3}$$

$$\Phi_{v}=-\frac{\Gamma}{2\pi}\theta$$

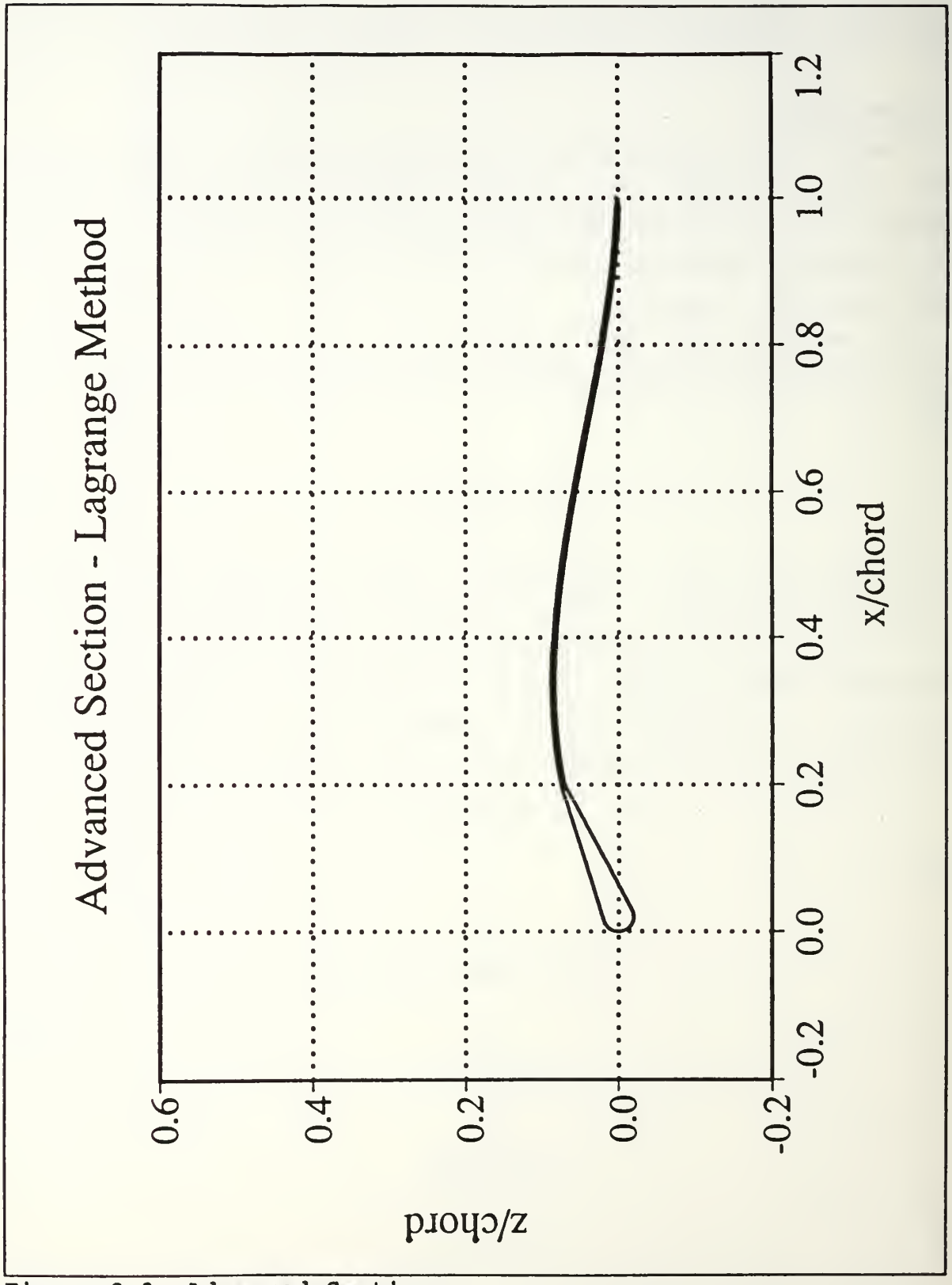

Figure 2.3 Advanced Section

If the airfoil section is decomposed into a set of **n** panels to describe the section, the flow field can be represented by the superposition of **n** sources located at the mid-panel points, a uniform flow and a constant vortex strength. Hence, the total number of unknowns is **n+1**.

By applying boundary conditions a solution to the system may be obtained. The flow tangency condition at the panel mid-points results in **n** equations. A final boundary condition is arrived at by applying the Kutta condition forcing the velocities of the upper and lower trailing edge panels to be equal. The system of elementary potential flows is now reduced to **n+1** equations and unknowns which can be expressed in matrix form:

$$[A][q]=[B]$$

where, **A** is the influence coefficient matrix, **q** is a column vector with the values of the **n** source strengths and the vortex strength. **B** is also a column vector equating the angular difference between the free stream angle of attack and the mid-point tangents and the wake condition.

The coding for a panel code is fairly straightforward but great care must be utilized in the geometry conventions used to specify the influence coefficient matrix. The code 'panel.f' contained in Appendix A was written by the author and adapted for use on sail sections. To adequately describe the irregular sections of interest a high number of panels was required with the upper limit currently 200. The airfoil shape is entered as an input file in one of two formats by the user. The input file can consist of standard **x,y** ordinates or be in the form of a two dimensional Plot-3D grid file. If a Plot-3d file is used the upper and lower trailing edge points along the **i** direction must also be provided.

From a computational standpoint, the main weakness in solving Laplace's equation occurs in the 'panel.f' code when inverting the **A** matrix. The thickness of the section and number of panels utilized have a strong effect on the error when inverting the influence coefficient matrix. The actual thickness of the sail

section is of the order of five mil's, a very small thickness, which is not realistic for the code's precision. Experience has shown 0.5% thickness to be a reasonable compromise. The complex geometries also suggest that a large number of point should be used to describe the section with 151 panels having been determined to be sufficient.

D. BOUNDARY LAYER CODES

The panel code provided the simplest method to obtain results for the pressure coefficient. Similarly, it is highly desirable to obtain viscous results in a simple and timely manner. Boundary layer codes represent the next logical step toward understanding the viscous behavior for the low Reynolds number present.

Two boundary layer codes were explored to investigate their suitability for sail analysis. The first of the codes, 'dbl2.f' a direct boundary layer code, was employed with very limited utility. The code employs a panel method routine to compute the pressure distribution which is then used to compute the boundary layer profiles. The second code utilized was the viscous invisid interaction code developed by Cebeci at McDonnell-Douglas Aircraft Company. This code carries the process used in the direct boundary layer code a stage further. After computing the boundary layer the code then adds the additional thickness of the viscous layer to the airfoil shape. This new effective shape is then run through the inviscid scheme again to compute a new boundary layer. This iterative routine is repeated until the change in the boundary layer becomes sufficiently small. The iterative boundary layer technique was nothing short of a total failure. This was due to the inability of the Smith-Hess panel routine used by the code to successfully handle the irregular sections. However, some insight into the flow separation characteristics was gained through this code.

It was hoped that these two codes or methods would be of great value as they represent the next order of sophistication above the simple potential inviscid solution. Both schemes proved to be a

disappointment toward the analysis of the sail shapes. While these codes work well for standardized airfoil shapes they proved to be of little value for the irregular shapes. Their failure is due to the fact that they do not handle separated flow regions well. Potential flow modeling of the highly irregular sail shapes produced large pressure perturbations which caused the boundary layer to separate in the numerical solution. After several attempts to improve on the solutions these methods were abandoned in favor of the Navier-Stokes and Euler methods.

E. EULER and NAVIER-STOKES METHOD

The Navier-Stokes (NS) equations represent the most robust tool currently in use in the field of computational fluid dynamics. The derivation of the NS equations and their CFD solution method will not be discussed because they are well documented in References 1 and 5. The two-dimensional vector form of the equations may be expressed as:

$$\frac{\partial Q}{\partial t}+\frac{\partial E'}{\partial x}+\frac{\partial F'}{\partial y}=0 \tag{2.4}$$

where,

$$Q=(\rho,\rho u,\rho v,e)^T$$

$$E'=\begin{matrix}\rho u\\ \rho u^2+p-\tau_{xx}\\ \rho uv-\tau_{xy}\\ (e+p)u-u\tau_{xx}-v\tau_{xy}+q_x\end{matrix}$$

$$F'=\begin{matrix}\rho v\\ \rho uv-\tau_{xy}\\ \rho v^2+p-\tau_{yy}\\ (e+p)v-v\tau_{yy}-u\tau_{xy}+q_y\end{matrix}$$

The Euler solution is readily obtained from the NS equations when the viscous terms are discarded.

The Navier-Stokes (NS) code used to examine the flow characteristics of the sail sections, 'ns2.f' was developed by Professor J. A. Ekaterinaris of the Navy-NASA Joint Institute of Aeronautics. Slight modifications to 'ns2.f' were made in the form of additional write statements to save unsteady motion solutions at regular time intervals and to simplify steady solution inputs. A call to the grid rotation subroutine was added to preclude the input of a rotated grid when running 'ns2.f'. The major features of the code are:

* Upwind differencing
* Baldwin-Lomax turbulence modeling
* Ability to restart the code

Navier-Stokes solutions were obtained after approximately four thousand iterations from a uniform flow field, based on the density residuals, Figure 2.4. Solutions could be obtained with a fraction of the four thousand iterations if a restart was initiated from a previous solution (example: an 8 degree angle of attack solution is used to compute a ten degree solution). The NS solutions were computed using the Iris Indigo work stations in the CFD laboratory. This required approximately twelve hours of CPU time for four thousand iterations using a 251 by 71 grid run with a Courant number of 2100. While this may seem to be a huge amount of computer time, it must be kept in mind that this was only a small work station and that few of the solutions required four thousand iterations by using the restart feature. Euler solutions can also be obtained from this code in a similar manner with the correct switches in the input file to discard the viscous terms.

F. GRID GENERATION

The need for a grid system to define a flow field around a body arises from the necessity of transforming from the physical domain to a discrete computational domain. The theory of grid generation will not be covered in this thesis. Merkle's text, Reference 5, explains this process as do several other texts in the

field of CFD. Grid generation for the section depicted in Figures 2.1 and 2.2 was accomplished utilizing the code 'hypgen'.

The grid type selected for this analysis was the 'C' grid

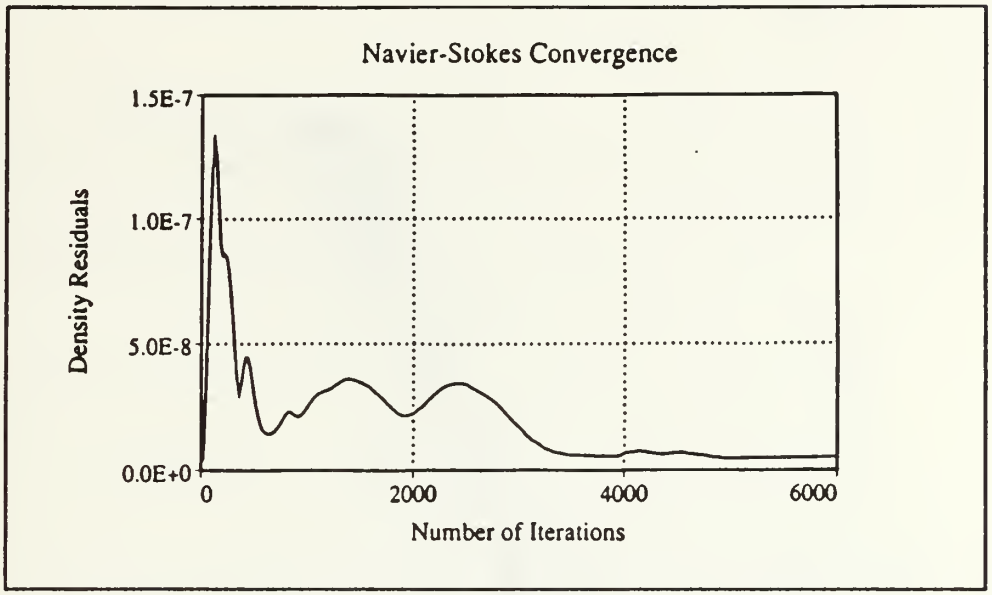

Figure 2.4 Navier-Stokes Solution Convergence

which is most commonly used for 2-dimensional airfoils. The 'C' is in reference to the shape or manner in which this type of grid is wrapped around the airfoil. The **i** stations are along the wake and airfoil directions while the **k** stations extend from the airfoil surface to the far field. The primary difficulty encountered was ensuring the orthogonality of the grid lines around the leading edge and forward portion of the sail sections. Additional points along the airfoil surface were added to the luff section to smooth the interval distance along the **i** direction near the leading edge. For the details in the grid generation software the 'hypgen' user manual should be consulted.

The full dimensions of the grids used are shown in Figure 2.5. These dimensions, 10 chords lengths ahead, above, below and 30 chord lengths aft of the sail section, were selected to ensure that solutions would smoothly match the far field boundary conditions. The grid used for the inviscid Euler solutions is shown, Figure 2.6. For the NS calculations the number of stations from the airfoil to the far field was increased from 41 to 71 station. This was done to accurately resolve the boundary layer near the airfoil

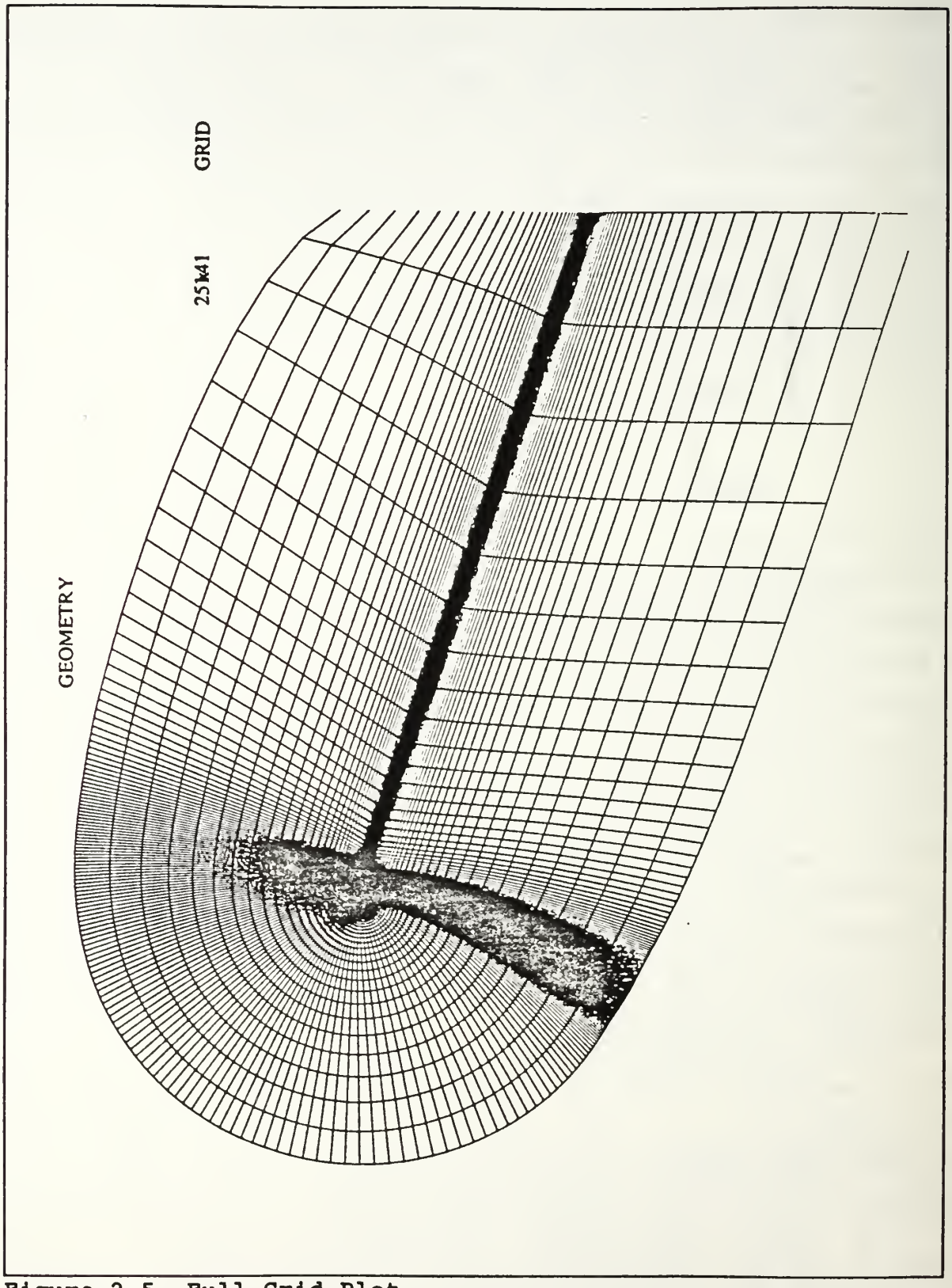

Figure 2.5 Full Grid Plot

surface. The increased resolution can be seen in Figure 2.7.

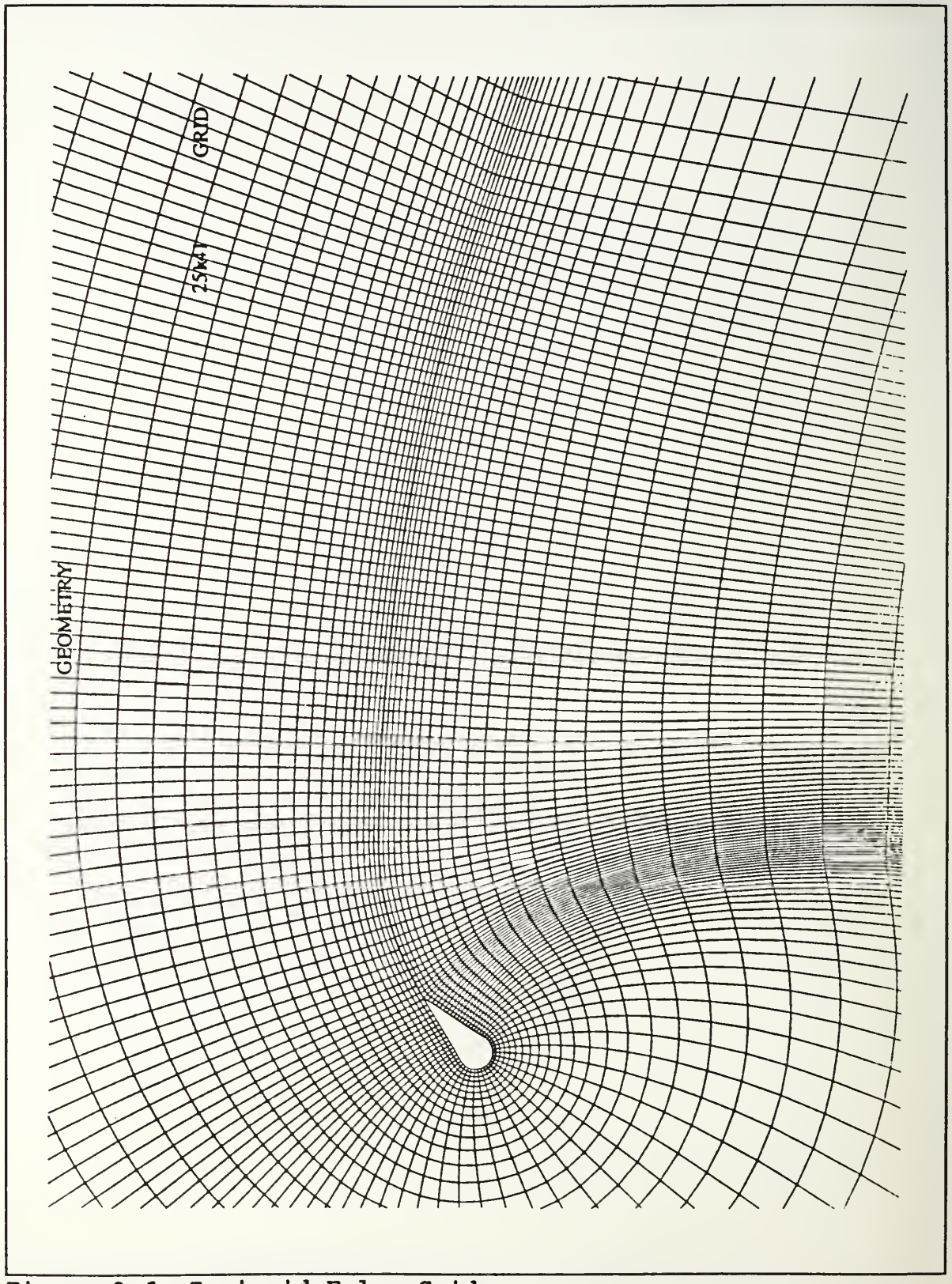

Figure 2.6 Inviscid Euler Grid

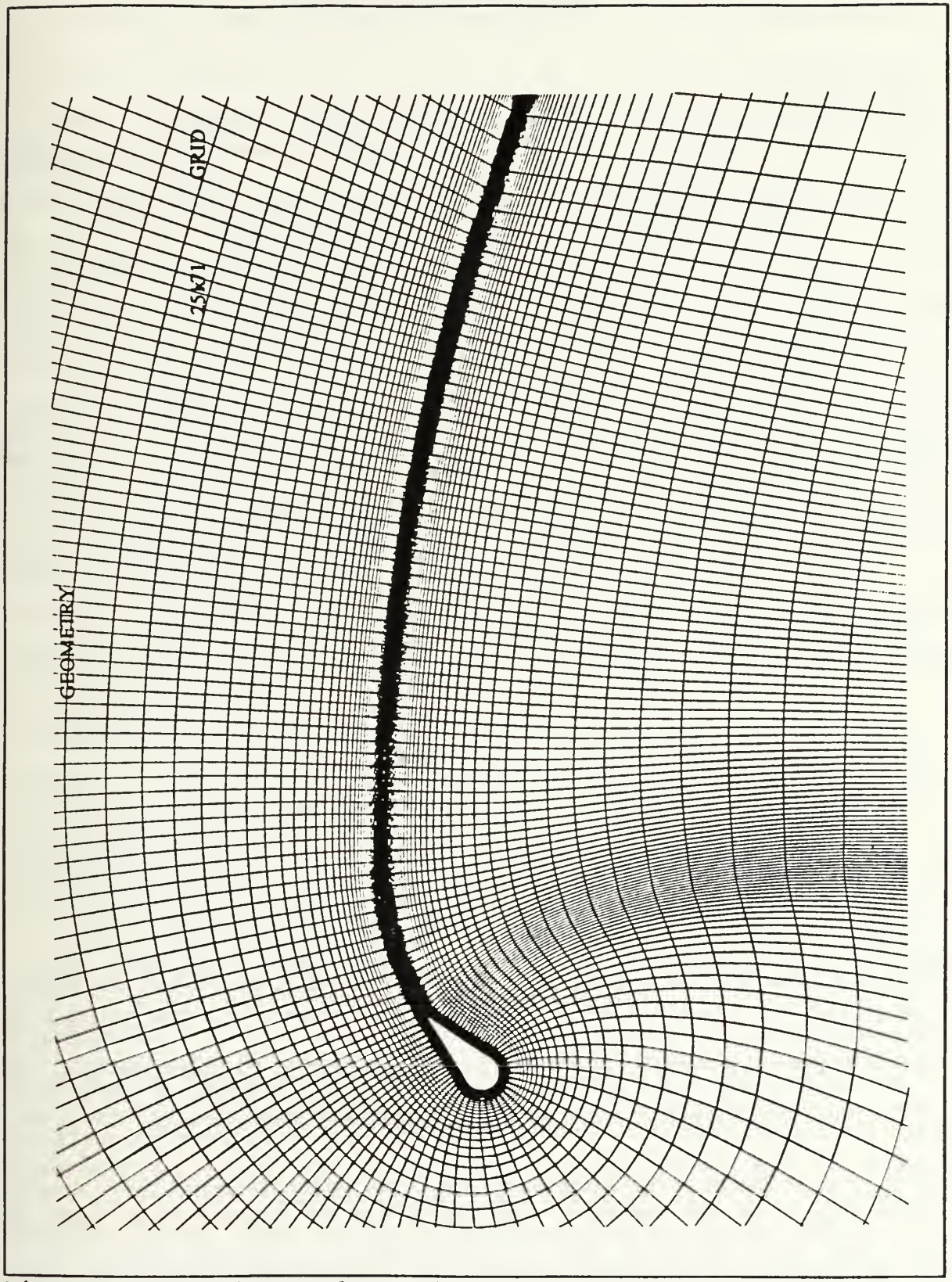

Figure 2.7 Navier-Stokes Grid

III. EXPERIMENTAL APPROACH

A. BACKGROUND

The most frequent criticism of computational fluid dynamic solutions is that they may not accurately reflect the actual flow present. It was therefore highly desirable to validate the computational work conducted with experimental data for the sections of interest. Investigations into previous work in this field failed to find an adequate description of the flow around windsurfing sail sections. The majority of the research conducted in this field has been for sail and rig combinations for specific yacht types. The wind tunnel experiments for this thesis were designed with the emphasis on predicting the separation regions present since this is the major challenge for viscous CFD methods.

B. WIND TUNNEL EXPERIMENTAL EQUIPMENT

The tunnel selected for carrying out the experiment was the 32 by 45 inch low speed wind tunnel located at NPS in Halligan Hall. The primary reason for the selection of this tunnel was that it is capable of sufficient velocities to run tests at the actual Reynolds numbers present in the sailing environment. The tunnel is also sufficiently large to allow for reasonably sized models. It was desired to mount the model sections vertically to take advantage of the large optical windows on the sides of the test sections for viewing tufts. In addition, by using the greater tunnel dimension perpendicular to the model rotation axis, the

blockage for the experiments was held to under twelve percent for a model of eighteen inch chord with up to eighteen degrees angle of attack. Reference 8 contains a detailed description of the tunnel and its use.

The next area addressed was the choice of materials to construct the models from. Particular attention was given to the fact that the airfoils to be tested have very thin sections over the majority of the chord. A conventional rigid model would have had to be constructed of metal or fiberglass/composite materials for the aft section and of wood for the mast and luff portions. This approach was considered but abandoned due to the complexity, cost and long lead times in building such models.

The other option was to assemble the model from the same materials as used on the actual sails. This approach simplified the model building process and allowed for easy modification of the models. The use of the same materials and construction techniques also precluded trying to simulate the roughness associated with the different fabrics, films and seams that exist on windsurfing sails.

After deciding to use actual 2-dimensional sails as models, a means to hold the sail and mount the sail in the test section was developed. A rig was designed and built of aluminum, as is depicted in Figure 3.1. This rig allows for the model to be in tension between the top and bottom rails to maintain the correct shape. The leading edge or simulated mast is formed by a 0.750 inch diameter steel tube. This is equivalent to a mast radius of 2.08 percent for the eighteen inch chord. The leading edge tube is

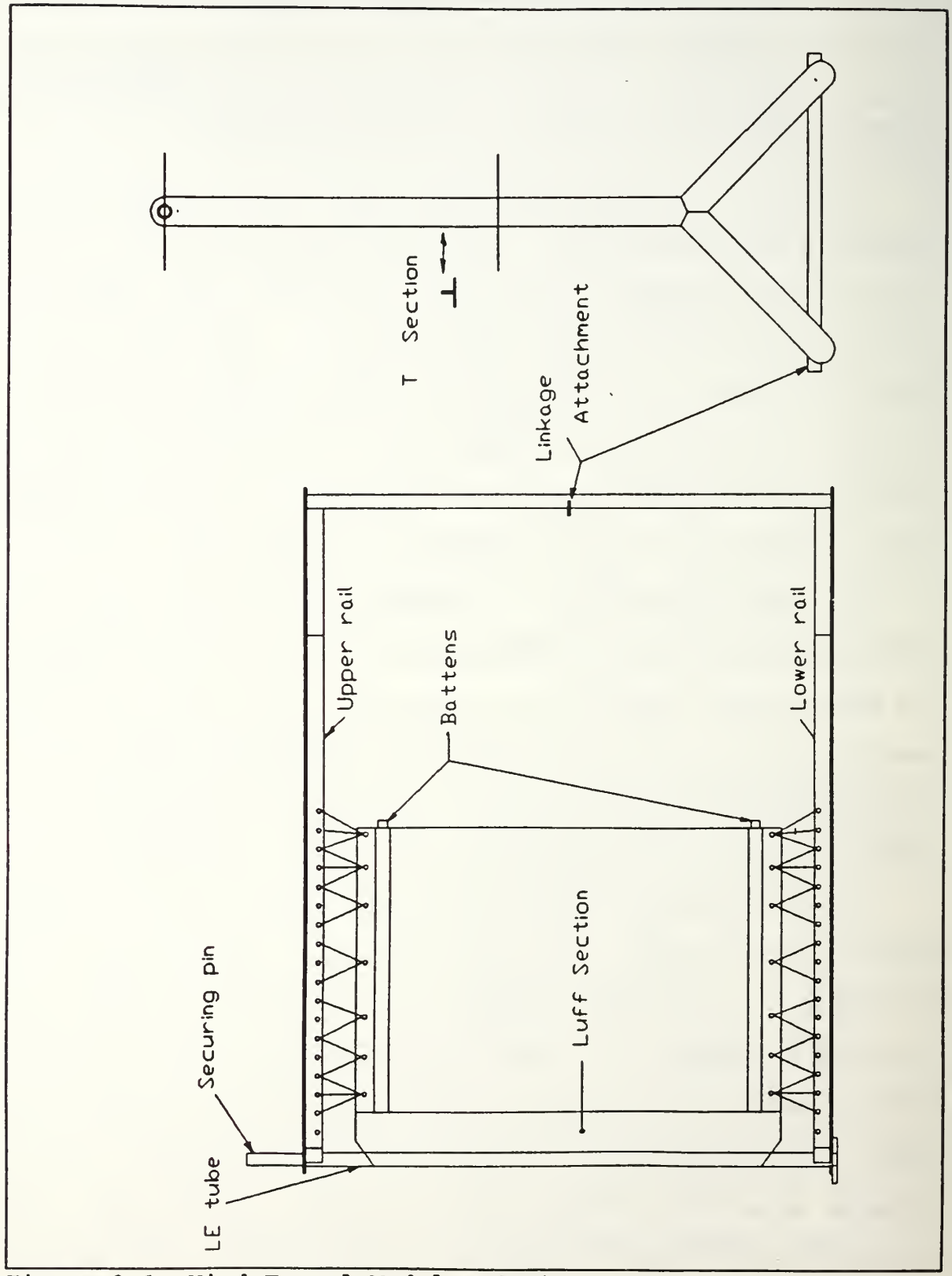

Figure 3.1 Wind Tunnel Model and Rig

freely supported and removable once the sail model is unrigged. This was designed to allow for the testing of several models without requiring a new rig.

Mounting the rig and model in the tunnel was accomplished by means of a pin that runs through the upper tunnel window, leading edge tube and rails, fitting into a flange mounted to the tunnel floor, Figures 3.2 and 3.3. This method did not require extensive modifications to the tunnel test section. A truss type structure downstream of the model was incorporated to provide a degree of torsional stiffness to the rig. The dimension of the truss aft of the leading edge was arrived at to coincide with the breather slot downstream of the test section. This allowed for the linkage controlling incidence to be placed through the breather slots.

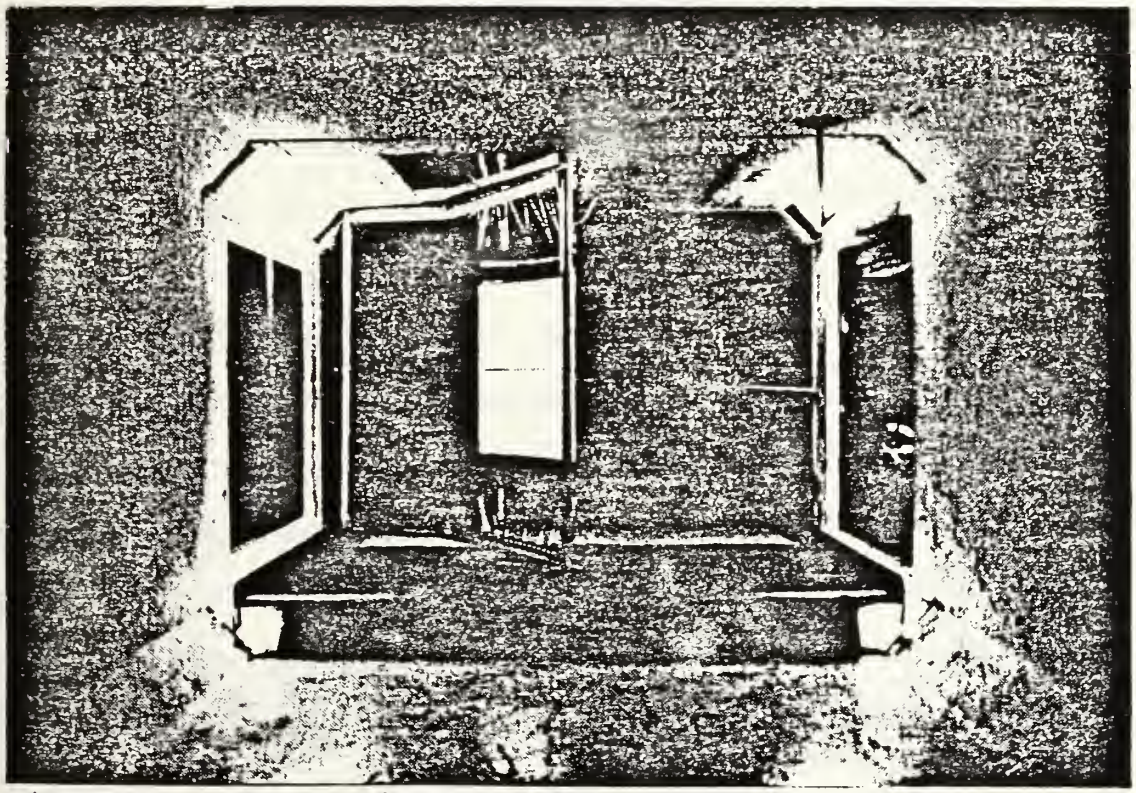

Figure 3.2 Front View of Model in Test Section

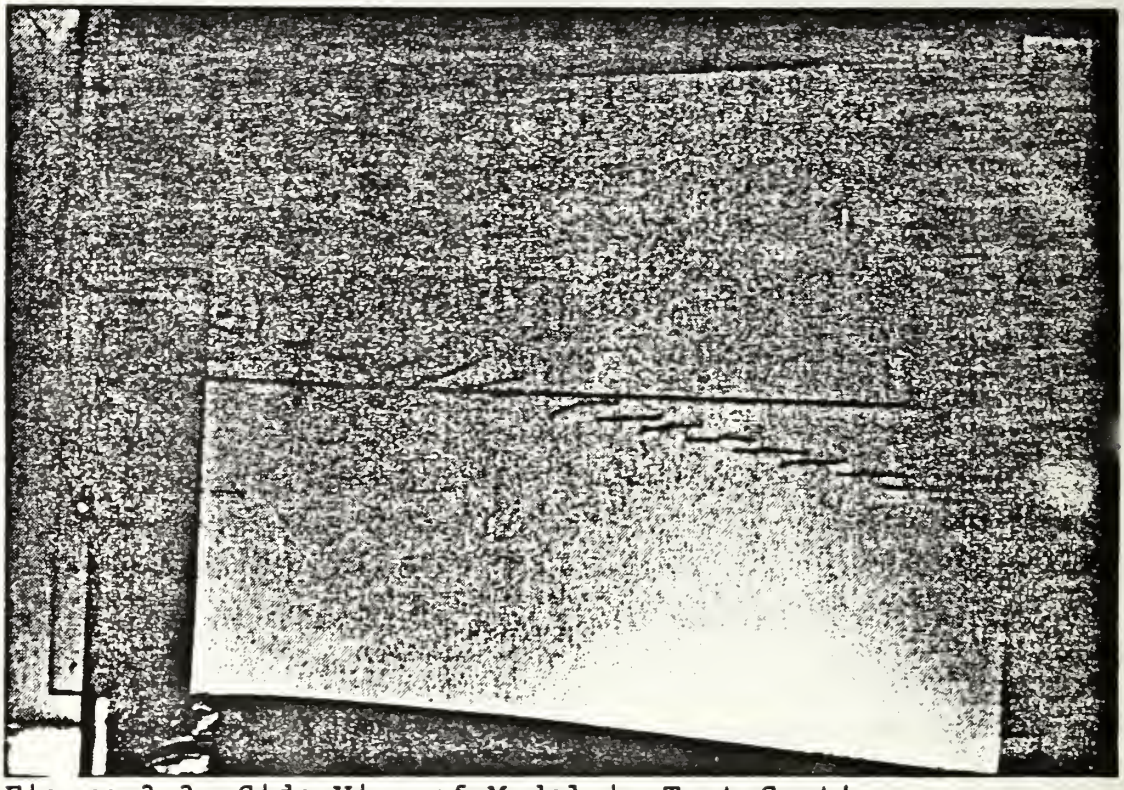

Figure 3.3 Side View of Model in Test Section

C. WIND TUNNEL MODEL CONSTRUCTION

The wind tunnel model that was used in the experiment was built and donated by Trevor Bayless at Waddell Sails in Santa Cruz. The materials incorporated are the same as those found on a high performance windsurfing sail. The leading edge luff segment was made of a durable dacron cloth while the aft section was made of a high modulus 7-mil mylar film sail material. A false seam was added to the leading edge to accurately pattern a seam that is present on actual sails. Areas beyond the body of the sail section were made with nylon strap material.

To build camber into a finished sail sailmakers use a combination of various panel layouts and full length battens held

in compression to form the final shape. For the tunnel model only battens could be used to form the section shape since the model is 2-dimensional. To force the airfoil shape into the desired shape preformed battens were used. The first set of battens, formed from 0.125 by 0.500 inch steel, were difficult to bend into the proper shape and were found to be too flexible for use. This difficulty was overcome with the use of carbon fiber - epoxy materials.

To build the carbon fiber battens, a female mold was first made of wood matching the desired camber less half the estimated thickness of the batten. The lamination used for the battens consisted of the following layers in an epoxy matrix:

1	6 ounce S-glass fiberglass
2	Carbon fiber reinforcing tape
1	0.125 inch balsa wood
2	Carbon fiber reinforcing tape
1	6 ounce S-glass fiberglass

The final battens proved to be very stiff and well worth the additional work.

D. FLOW VISUALIZATION

The primary means of observing the flow field around the section consisted of a series of tufts and a smoke stream. A number of different tuft materials and configurations were tried. Tape and cloth were placed over the lacing, used to tension the model, to cover the ends of the model to the rails. Flow along the center section was judged to be adequate for the experiments with

this configuration. The best tufts were determined to be very fine black thread with back lighting for photographs through the side windows.

The smoke flow was best observed through the upper window with flood lighting from the side windows. Reference 8 may be consulted for additional information concerning flow visualization. The smoke wand used in the 32 by 45 inch tunnel was lengthened by approximately two feet to minimize the growth of the flow prior to reaching the test section. It was noted that the smoke flow behavior was sensitive to the tunnel velocity. Velocities were limited to the range of 30 feet per second for this portion of the experiments.

IV. RESULTS

A. COMPARISON OF THE COMPUTED PRESSURE DISTRIBUTIONS

The first area examined was comparison of the computed pressure coefficient (**Cp**) distributions computed by the various methods. The panel method was found to be particularly sensitive to the thickness of the aft sections. It was desirable to keep the thickness value as small as possible to model the actual physical sections. However, the minimum feasible value was found to be half a percent of the chord length. The Navier-Stokes solution would have worked for any thickness but a value of 0.1 percent was used to be of the same order as in the panel method. Figure 4.1 is a pressure coefficient vs x/c plot from the panel code for the 11.5 % camber section at ten degrees incidence.

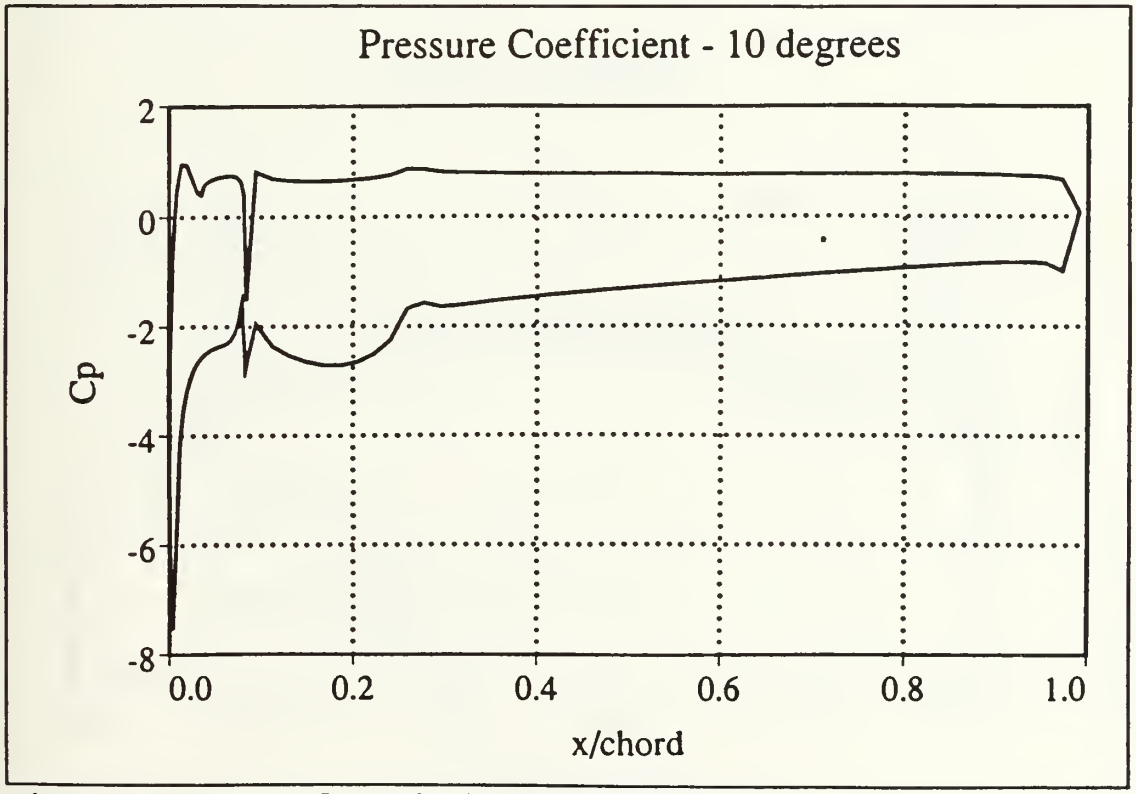

Figure 4.1 Panel Method Pressure Plot

The abrupt changes in the **Cp** aft of the immediate leading edge are caused by the change in curvature, from the flat section at the luff to the second order polynomial curve at 8.5 % and at the transition to the circular arc section occurring at 26.5 %. The poor convergence of the pressure at the trailing edge is due to the wedge shape trailing edge.

A comparison of the computed pressure using the panel, Euler and Navier-Stokes methods is depicted in Figure 4.2 for ten degrees incidence. The difference in the predicted **Cp** approximately one third aft of the leading edge on the lower surface using the Euler code is caused by the recirculating flow region. A vector plot of velocities for this region predicted by the Euler calculations is depicted in Figure 4.3 while the Navier-Stokes vector plot is shown in Figure 4.4.

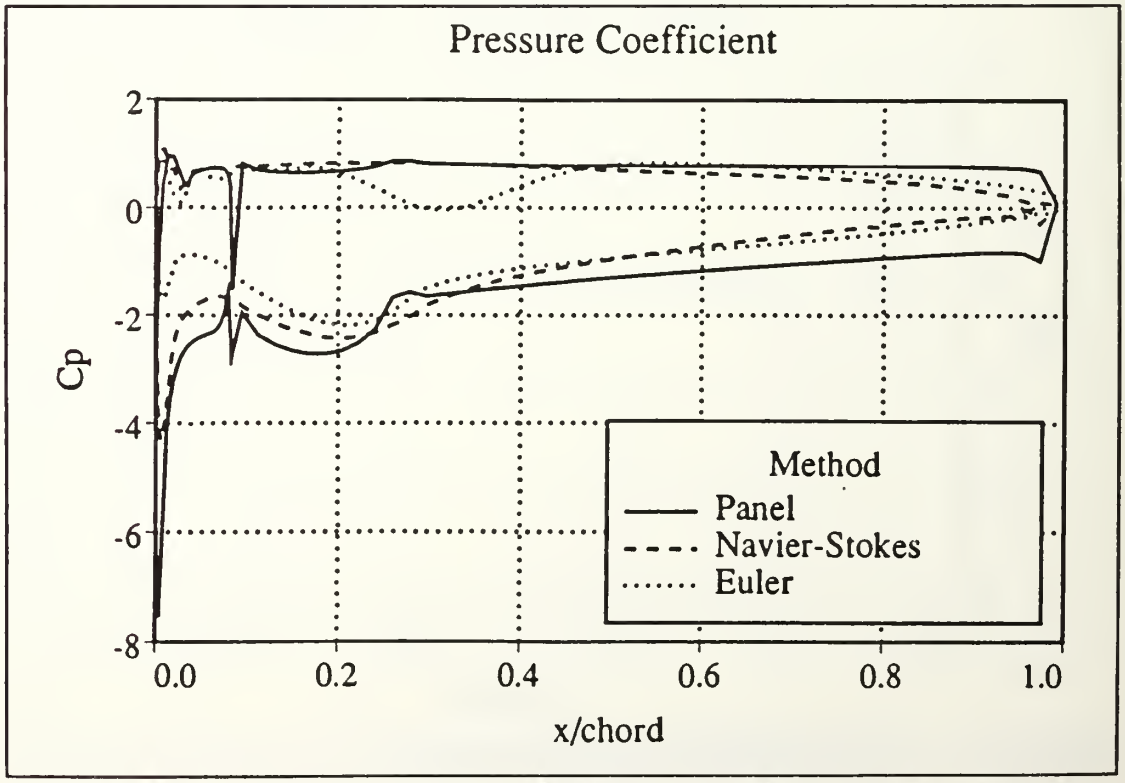

Figure 4.2 Pressure Plot of Panel, NS and Euler Methods

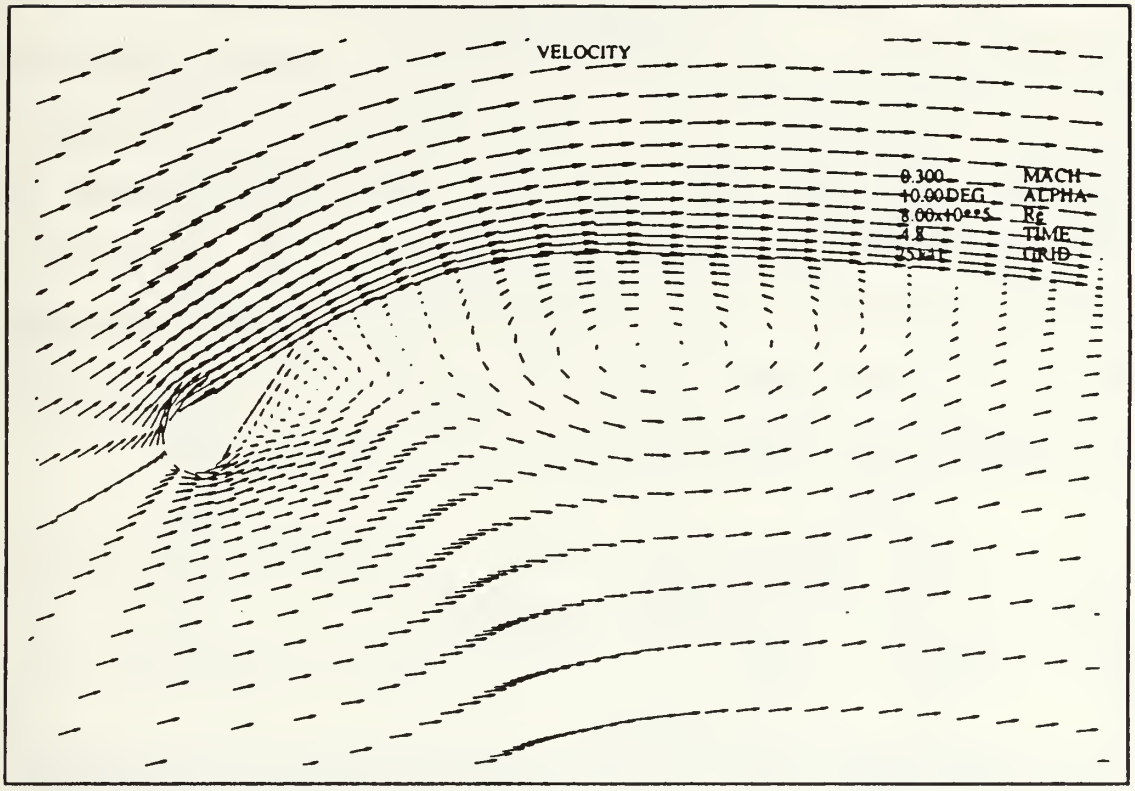

Figure 4.3 Euler Velocity Plot

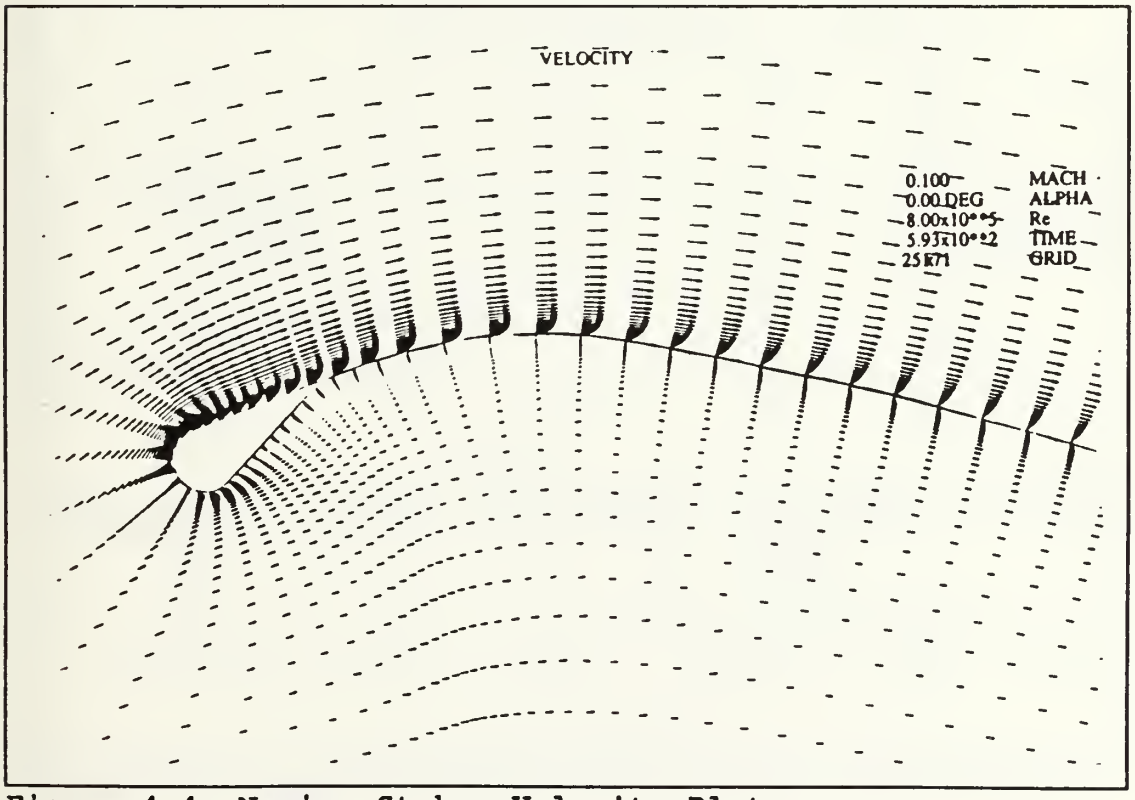

Figure 4.4 Navier-Stokes Velocity Plot

As the incidence angle is increased the differences between the inviscid panel code solutions and the viscous Navier-Stokes predictions can be discerned. It can be seen from Figures 4.5 though 4.7 that near stall the panel code is no longer valid. Figures 4.8 through 4.10 show the pressure field contours around the section computed by the Navier-Stokes code. The high number of contours around the mast radius demonstrates the importance of the large gradients and their effect on the stall behavior.

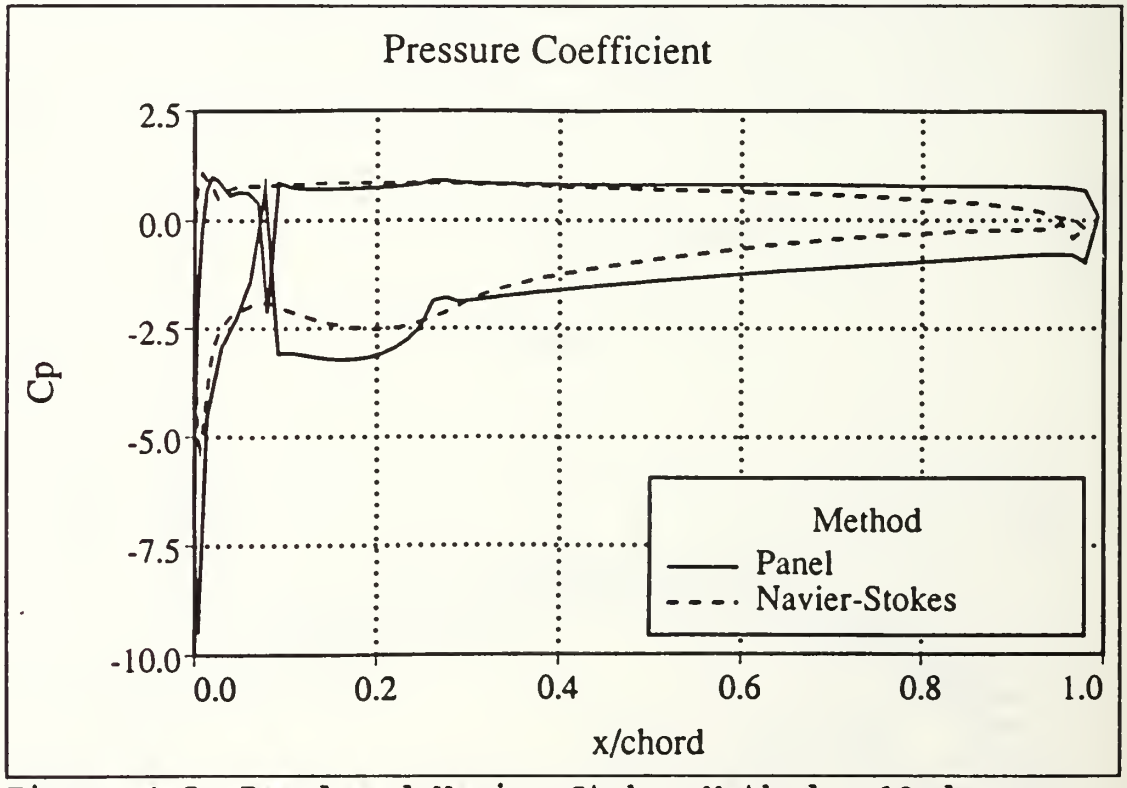

Figure 4.5 Panel and Navier-Stokes Method - 12 degrees

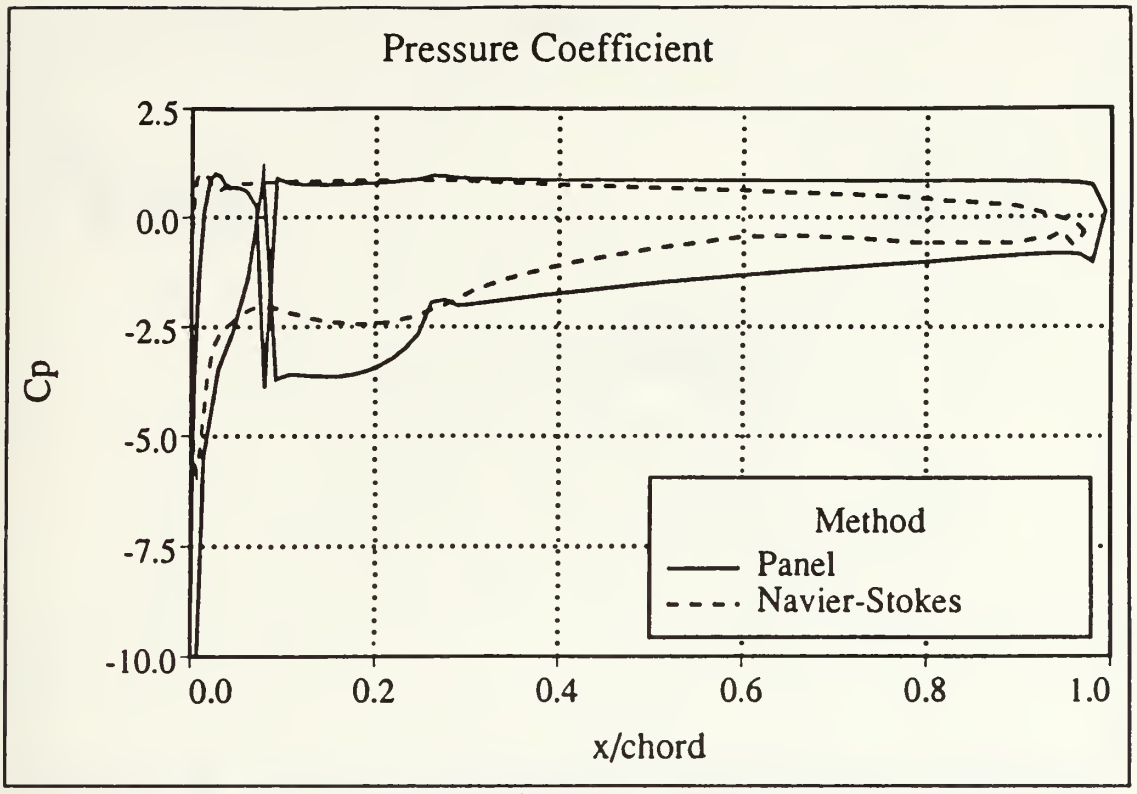

Figure 4.6 Panel and Navier-Stokes Plot - 14 degrees

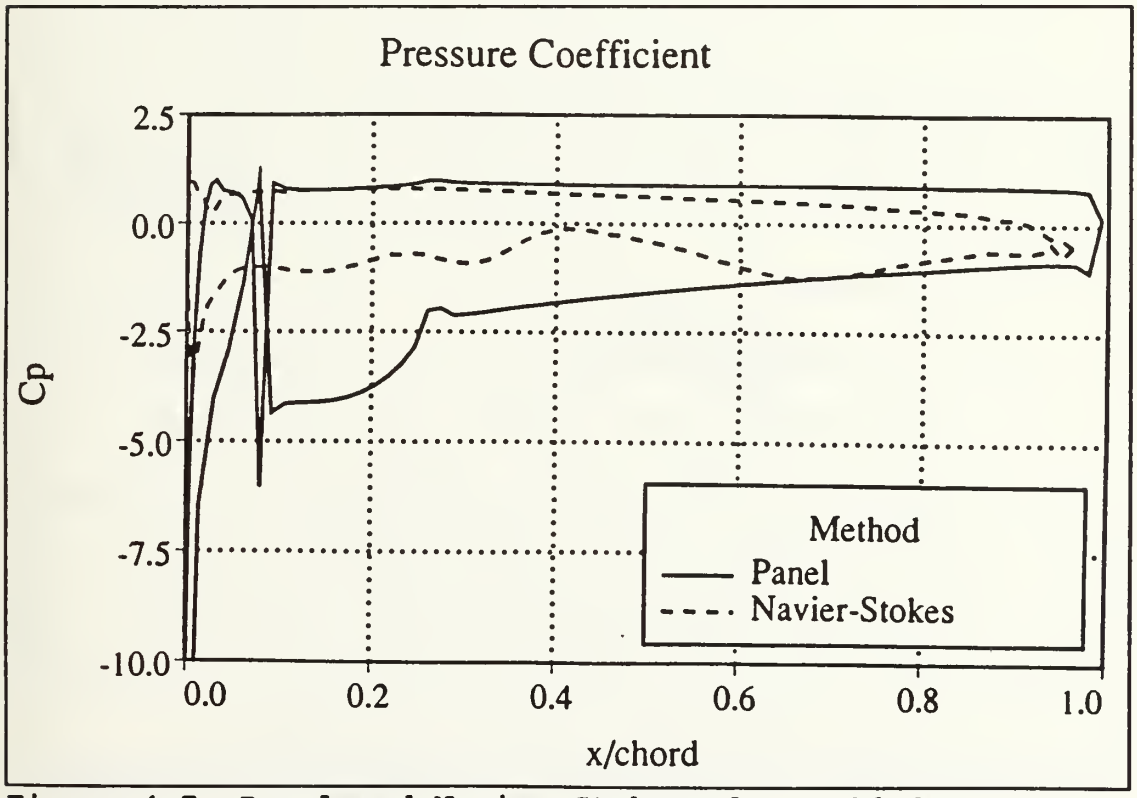

Figure 4.7 Panel and Navier-Stokes Plot - 16 degrees

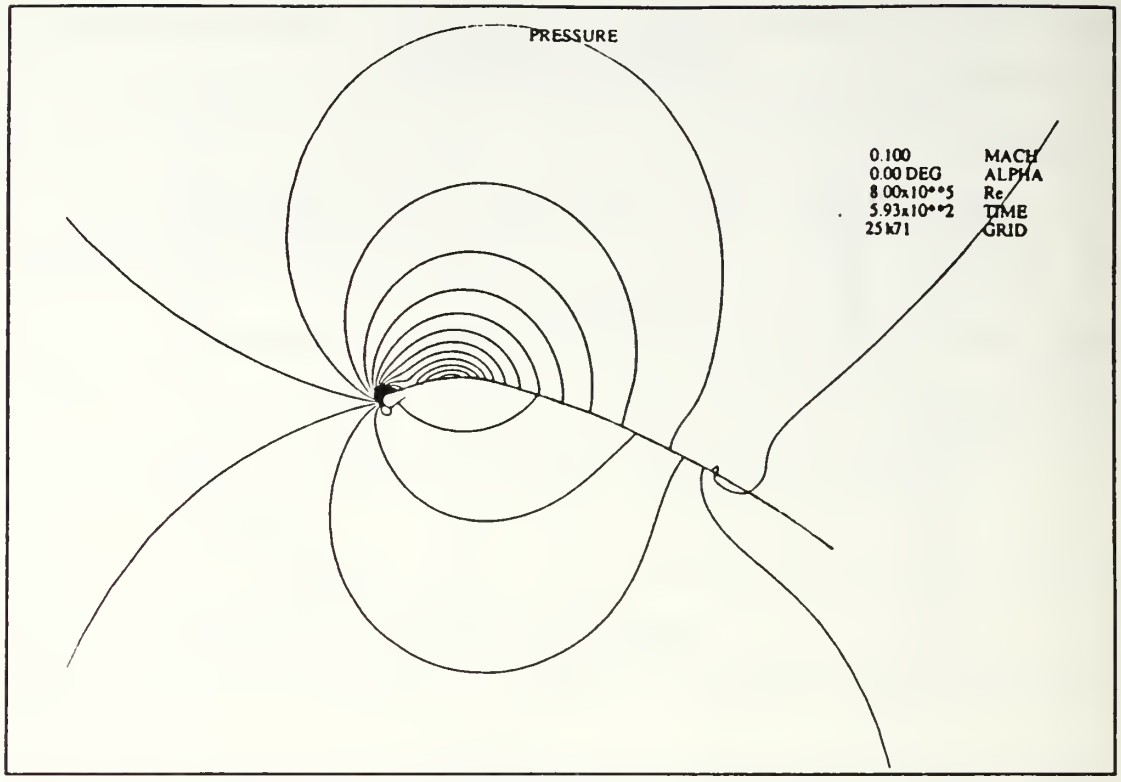

Figure 4.8 Navier-Stokes Pressure Contours - 12 degrees

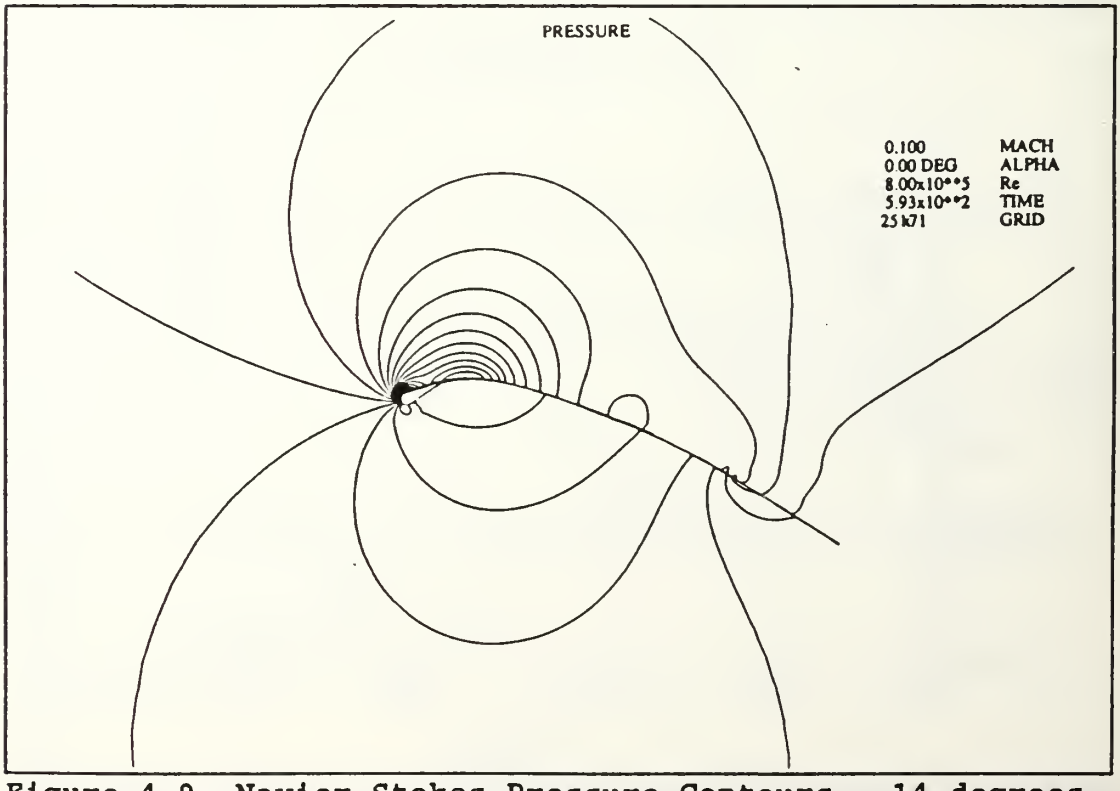

Figure 4.9 Navier-Stokes Pressure Contours - 14 degrees

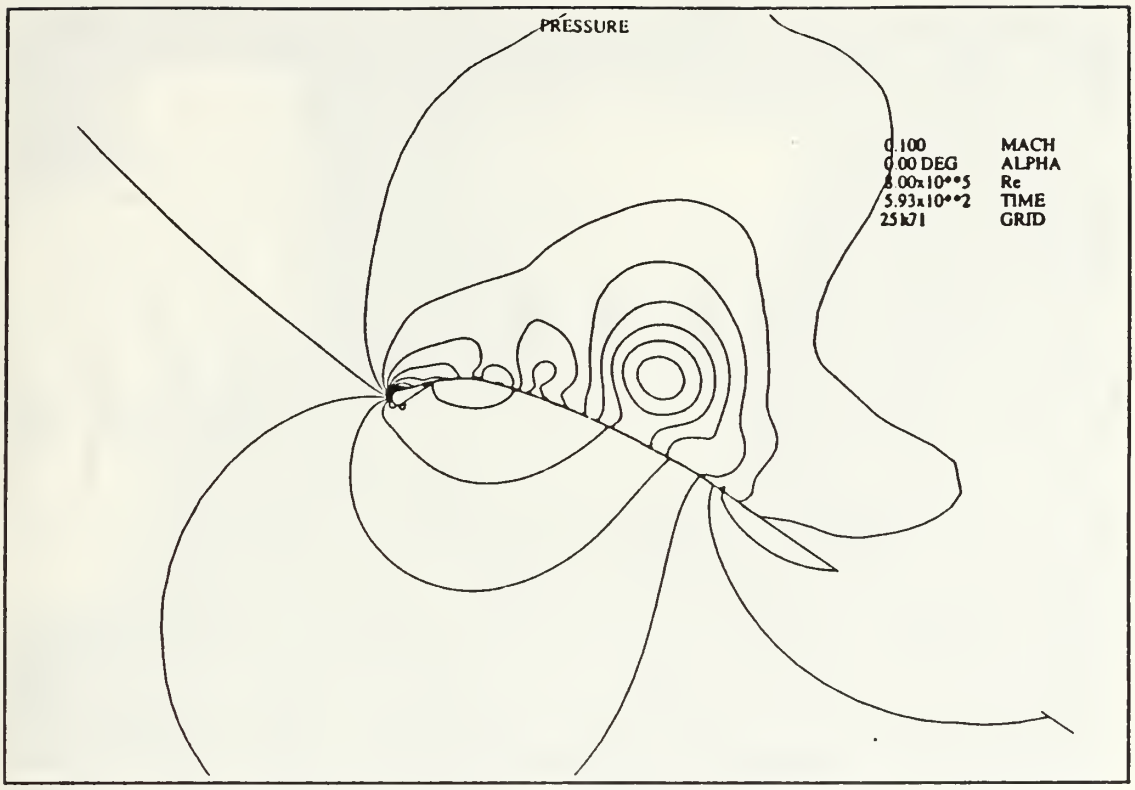

Figure 4.10 Navier-Stokes Pressure Contours - 16 degrees

B. VELOCITY VECTOR PLOTS

Several significant phenomena can be observed by examining the velocity vectors plots. At angles of attack below eight degrees a well defined separation and reversed flow region was predicted in the area near the lower luff with the Navier-Stokes code. The Euler code also predicted recirculating flow but estimated the region to be significantly larger and to be located further aft. The reversed flow region was first observed in the wind tunnel by means of the tuft survey. The size of the reversed flow region predicted by NS was verified by smoke flow at an angle of attack of four degrees. Figures 4.11 through 4.13 show this behavior by means of the NS prediction, smoke flow, and tufts, respectively.

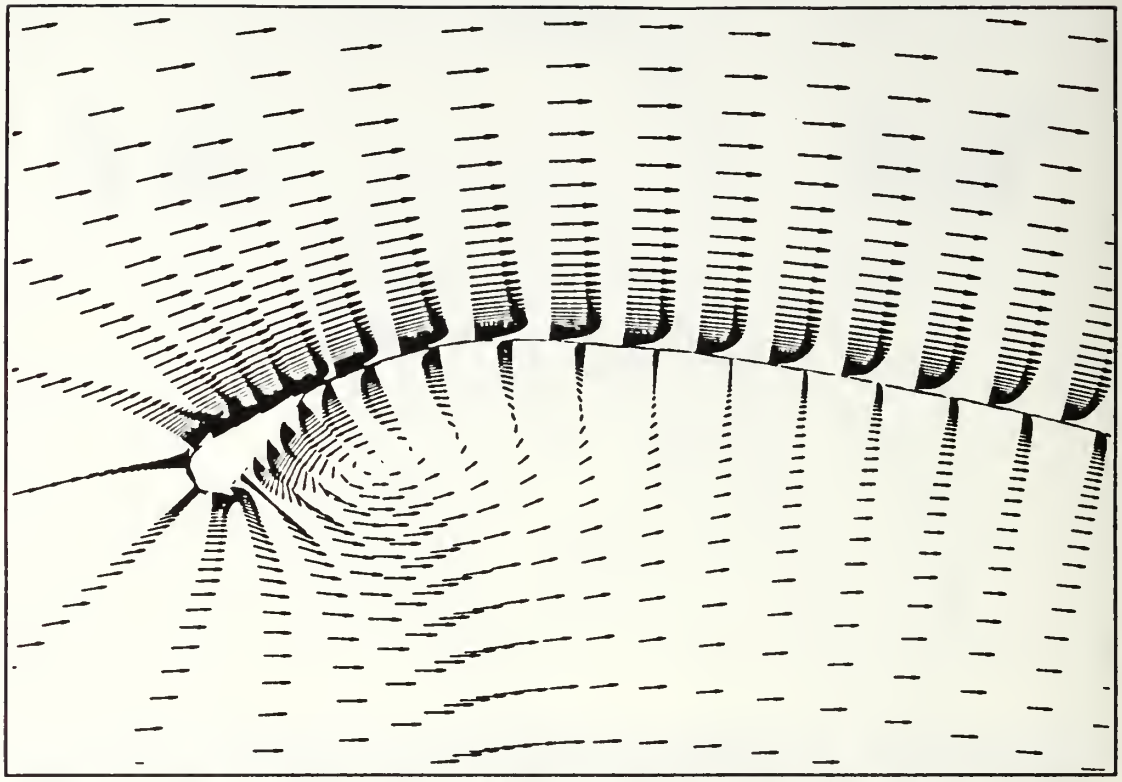

Figure 4.11 Navier-Stokes Prediction - 4 degrees

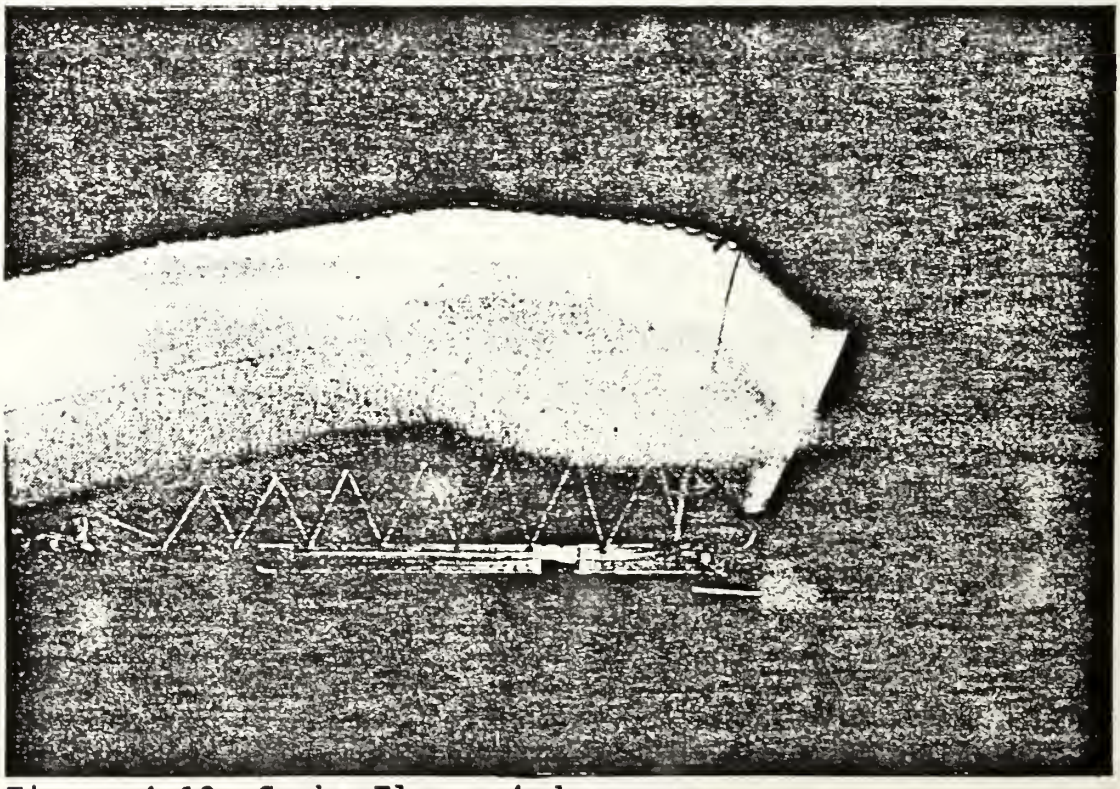

Figure 4.12 Smoke Flow - 4 degrees

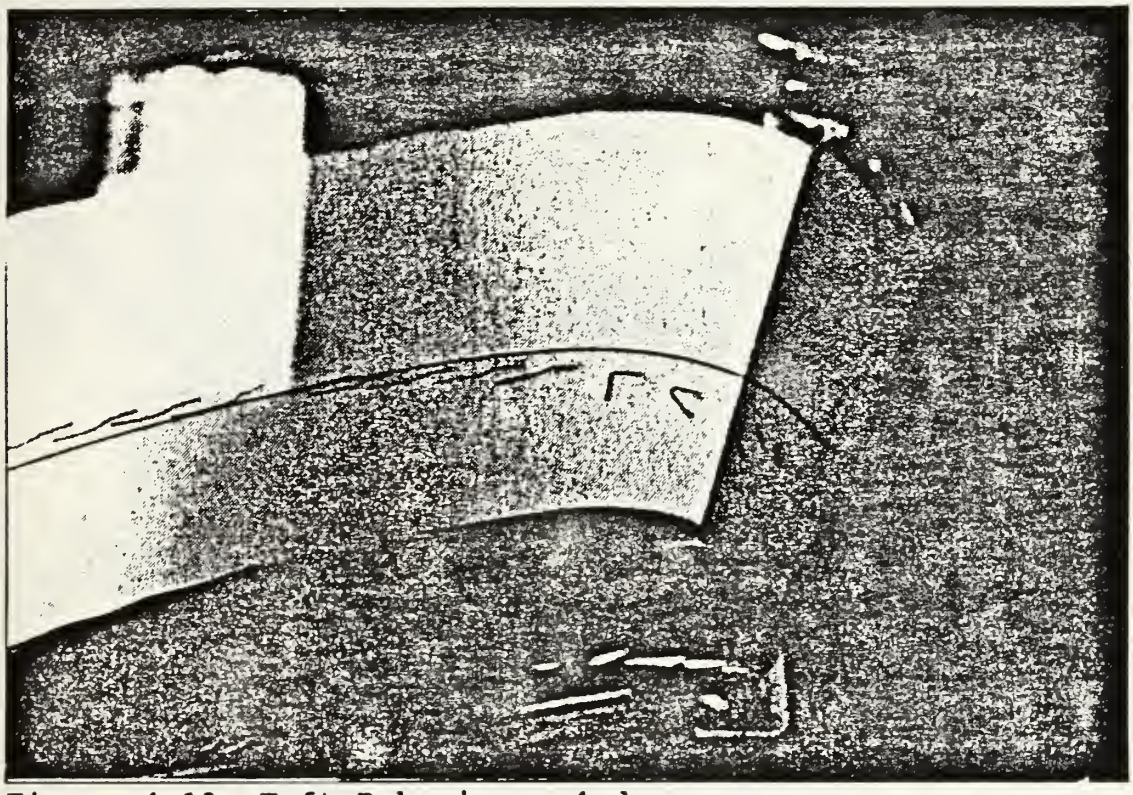

Figure 4.13 Tuft Behavior - 4 degrees

At angles of attack approaching stall a small separated flow region was predicted on the upper surface around the mast. This region is noteworthy because the flow quickly reattached to the flat luff segment and did not cause the entire upper surface to separate. This separation bubble was not visible during the flow visualization experiment, nor was this surprising. Viewing the bubble was highly unlikely due to its very small size. This prediction is pictured in Figure 4.13.

A major goal in the flow visualization effect was to precisely identify the stall angle. It was observed, however, that the section did not stall abruptly in a manner characteristic of thin airfoil sections. The flow near the surface appeared to slowly become more turbulent until reversing around fifteen degrees.

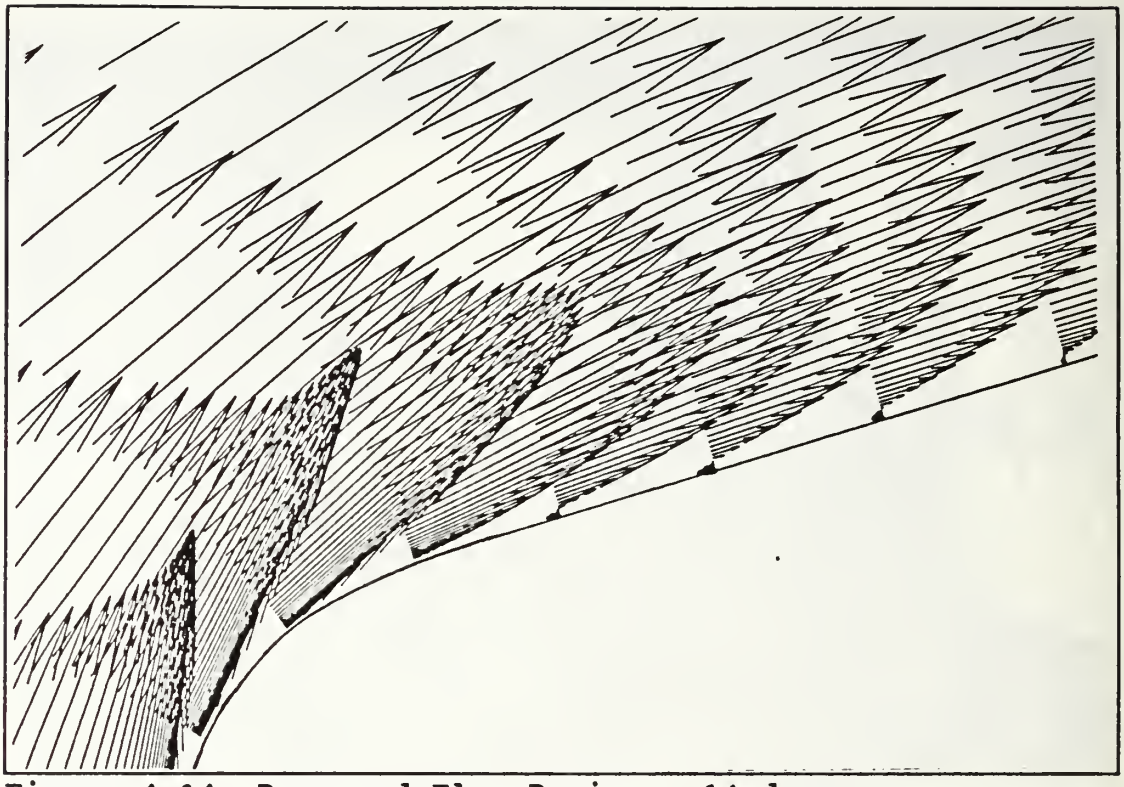

Figure 4.14 Reversed Flow Region - 14 degrees

This is an approximate angle due to the highly turbulent and random nature of the flow. The Navier-Stokes solutions show the boundary layer growing in thickness as the incidence is increased through fourteen degrees. This boundary layer growth is shown in Figures 4.15, 4.17,and 4.19 with accompanying tuft photographs in Figures 4.16, 4.18, and 4.20.

C. UNSTEADY MOTION

To increase the lift of sails windsurfers frequently use an oscillatory motion to increase the maximum lift generated by the sail. An effort to understand this phenomena was made using the unsteady options in 'ns2.f'. Several simulations were made with the test airfoil but only one solution will be presented. To simulate

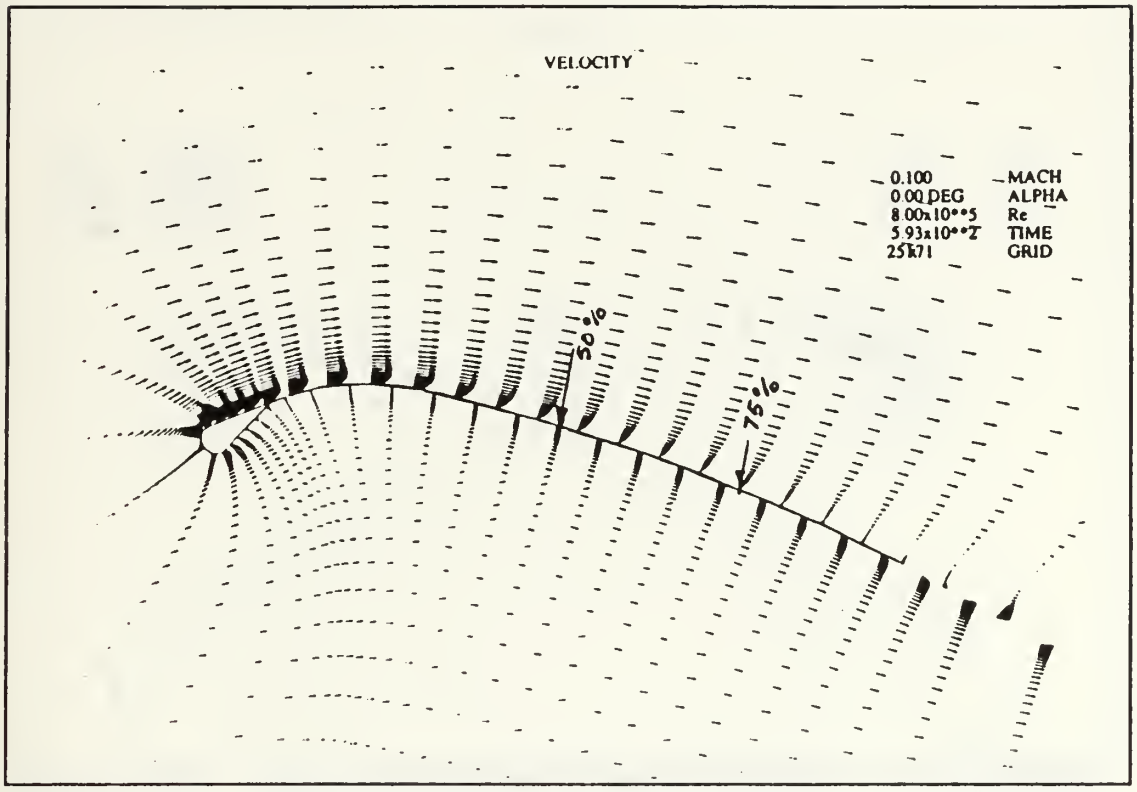

Figure 4.15 Navier-Stokes Velocity Vectors - 12 degrees

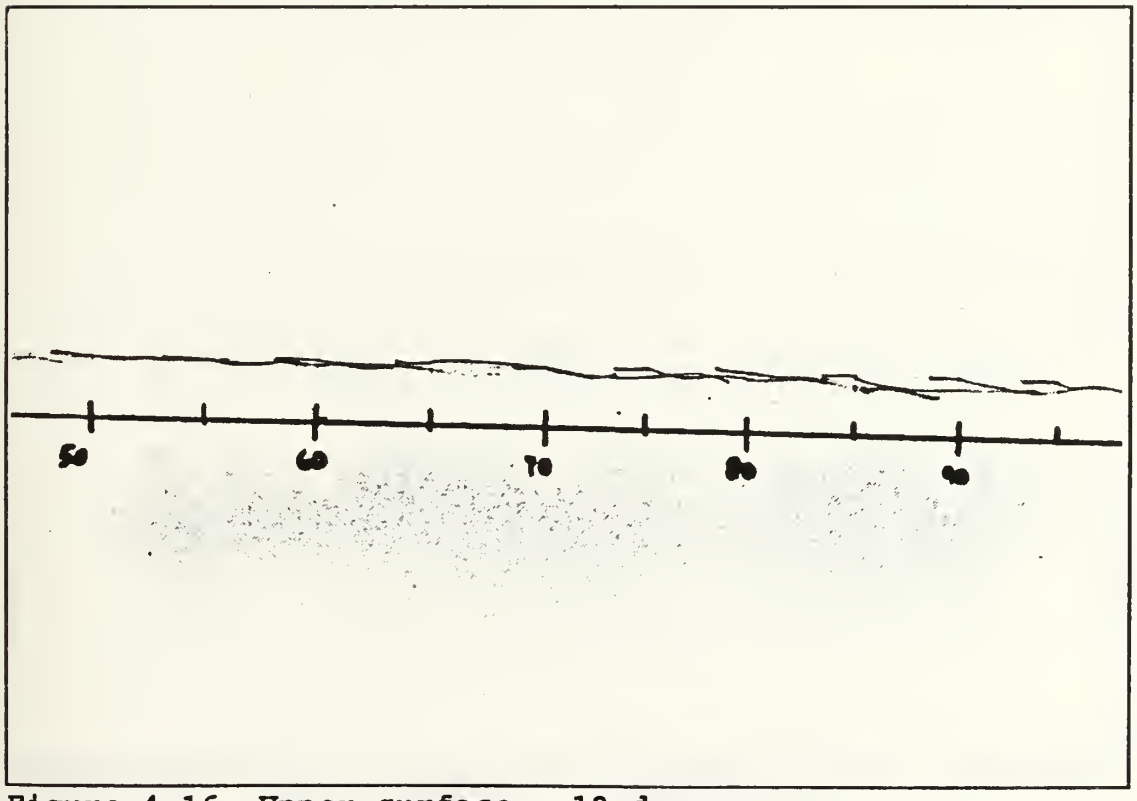

Figure 4.16 Upper surface - 12 degrees

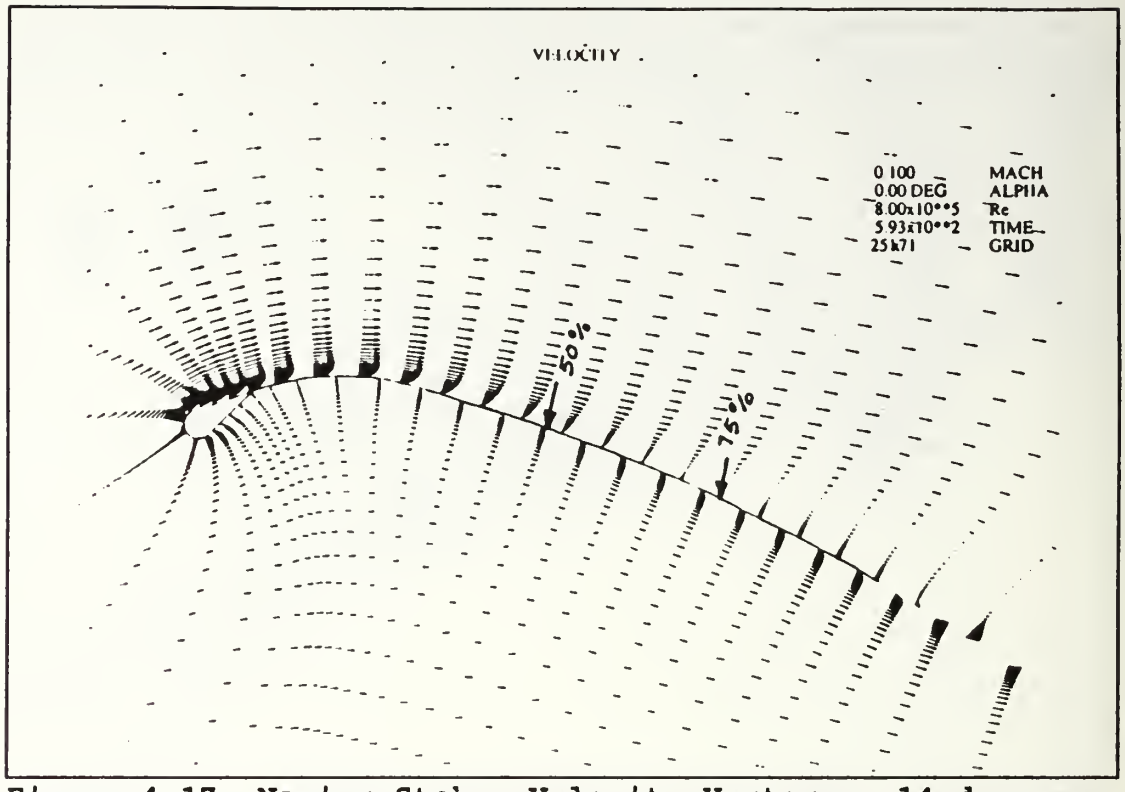

Figure 4.17 Navier-Stokes Velocity Vectors - 14 degrees

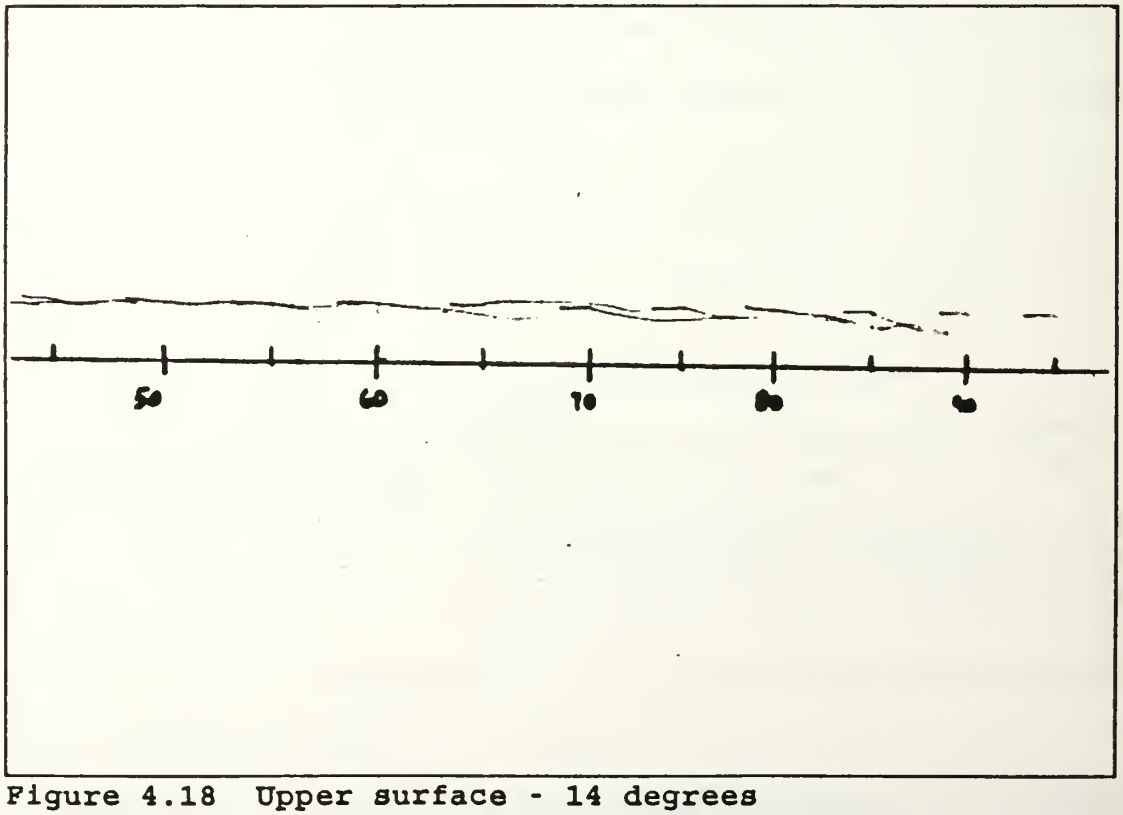

Figure 4.18 Upper surface - 14 degrees

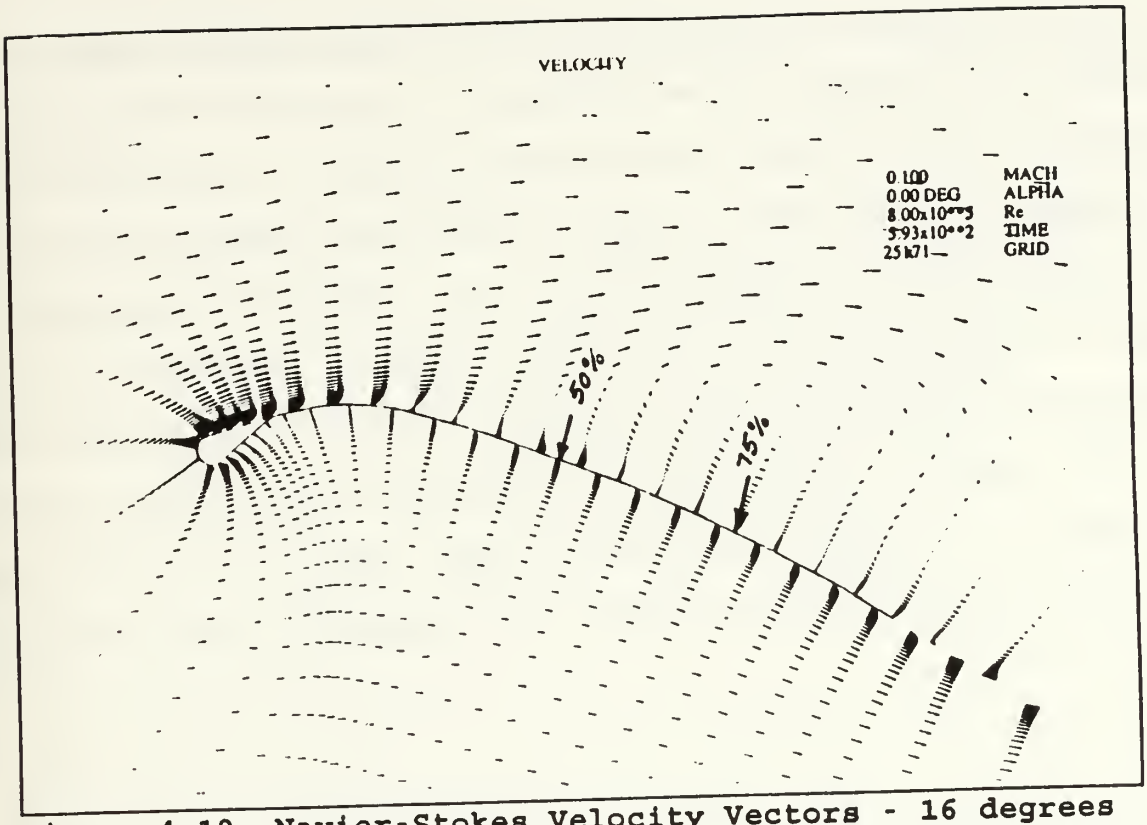

Figure 4.19 Navier-Stokes Velocity Vectors - 16 degrees

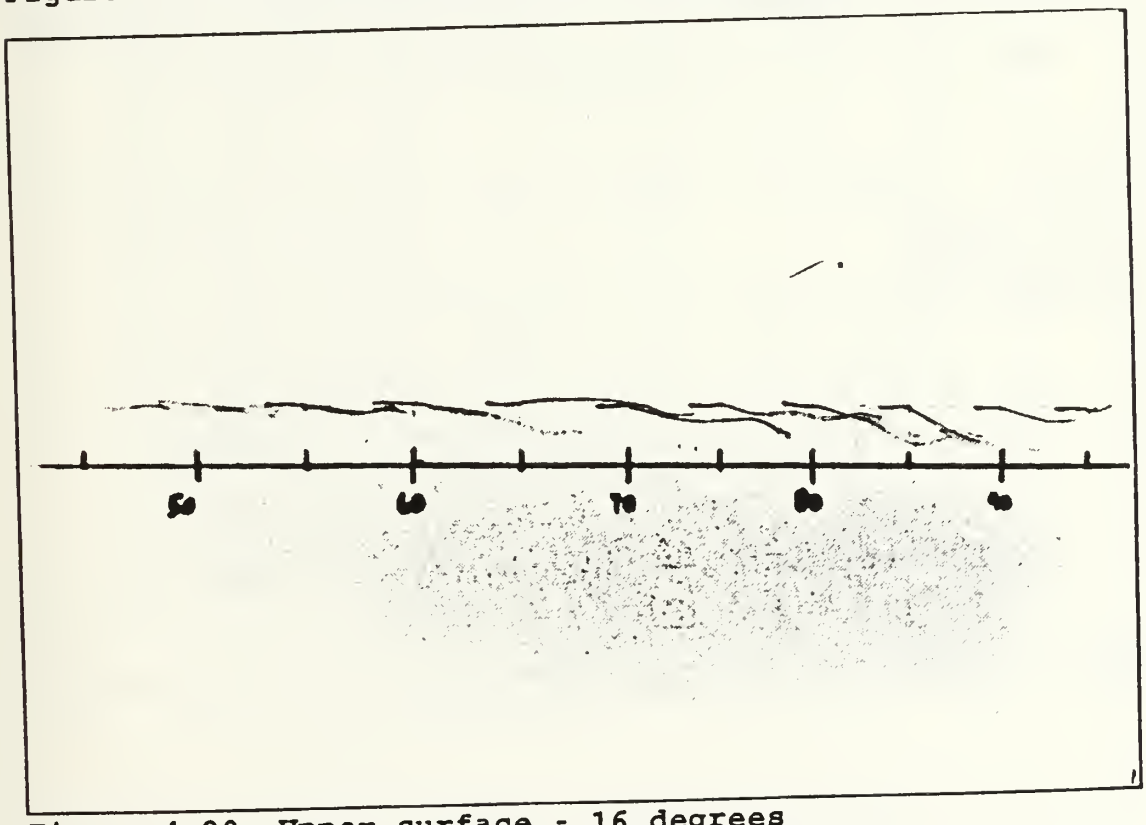

Figure 4.20 Upper surface - 16 degrees

the sailors actions a sinusoidal motion of four degree about a mean incidence of fourteen degrees was used. The reduced frequency was estimated to be 0.19 for an oscillation with a 1.5 second period. The code is started from a steady solution for time equal zero with a frequency shift of minus one half pi. The motion simulated is shown in Figure 4.21 as a function of time. The velocity field that results from the motion is shown in Figure 4.22 through 4.26.

The velocity vectors for the simulated motion show attached flow beyond the steady motion stall angle. The flow in fact stays attached through eighteen degrees but separates after the motion starts down.

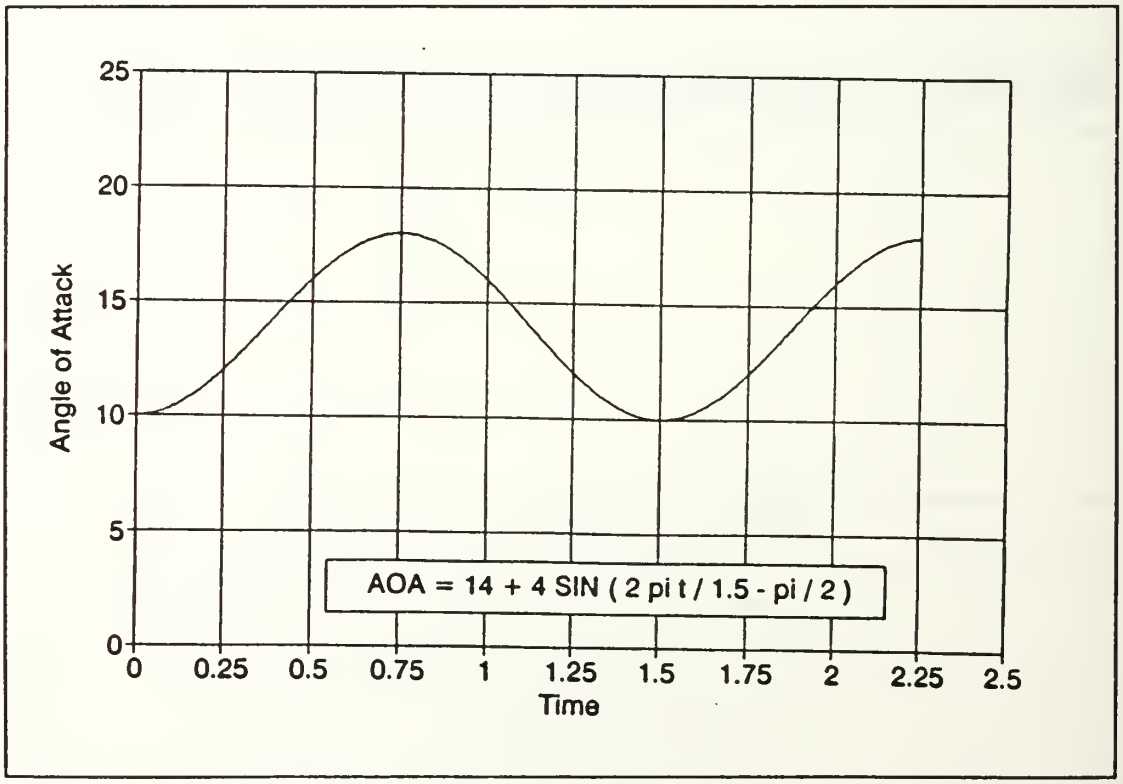

Figure 4.21 Unsteady Motion Simulation

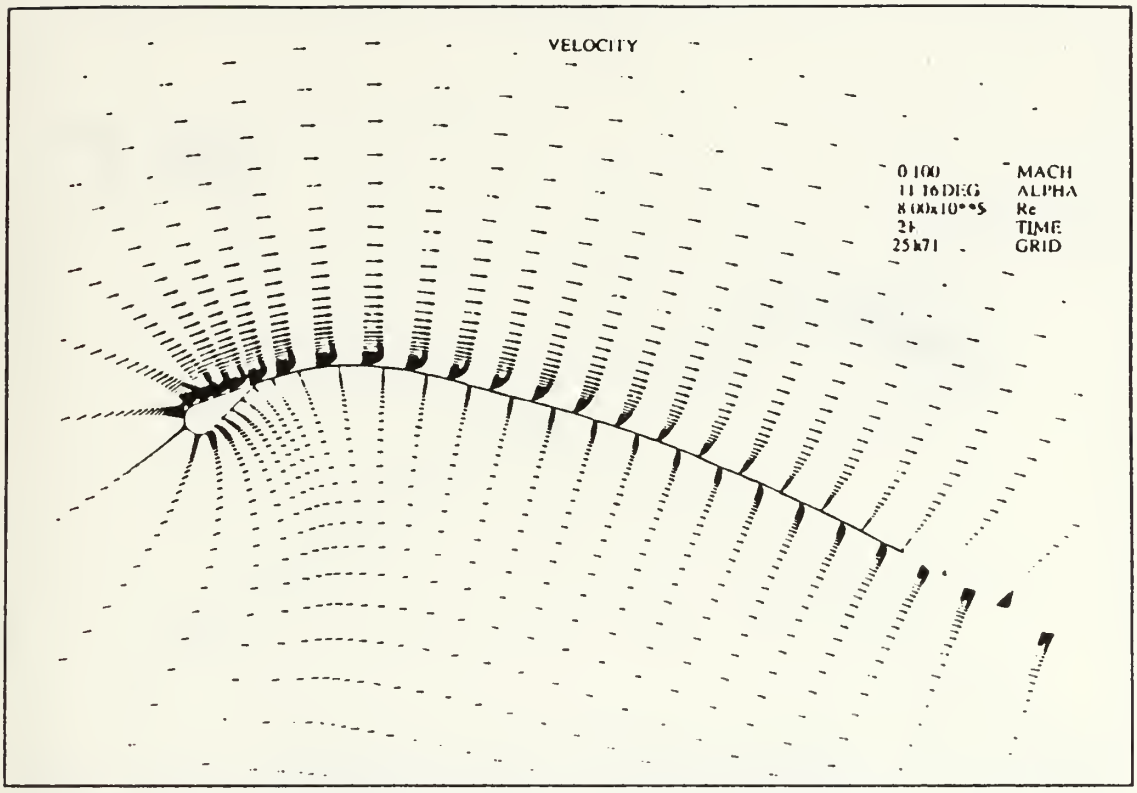

Figure 4.22 Unsteady Motion - 11.16 degrees

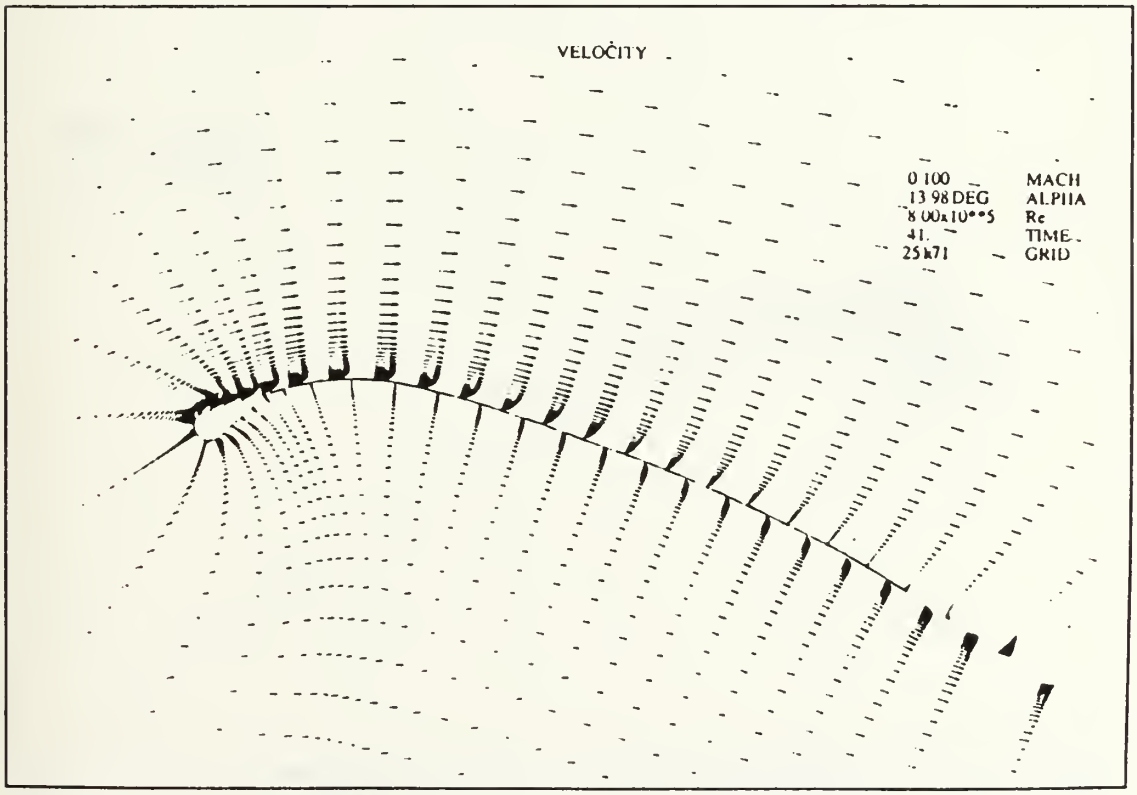

Figure 4.23 Unsteady Motion - 13.98 degrees

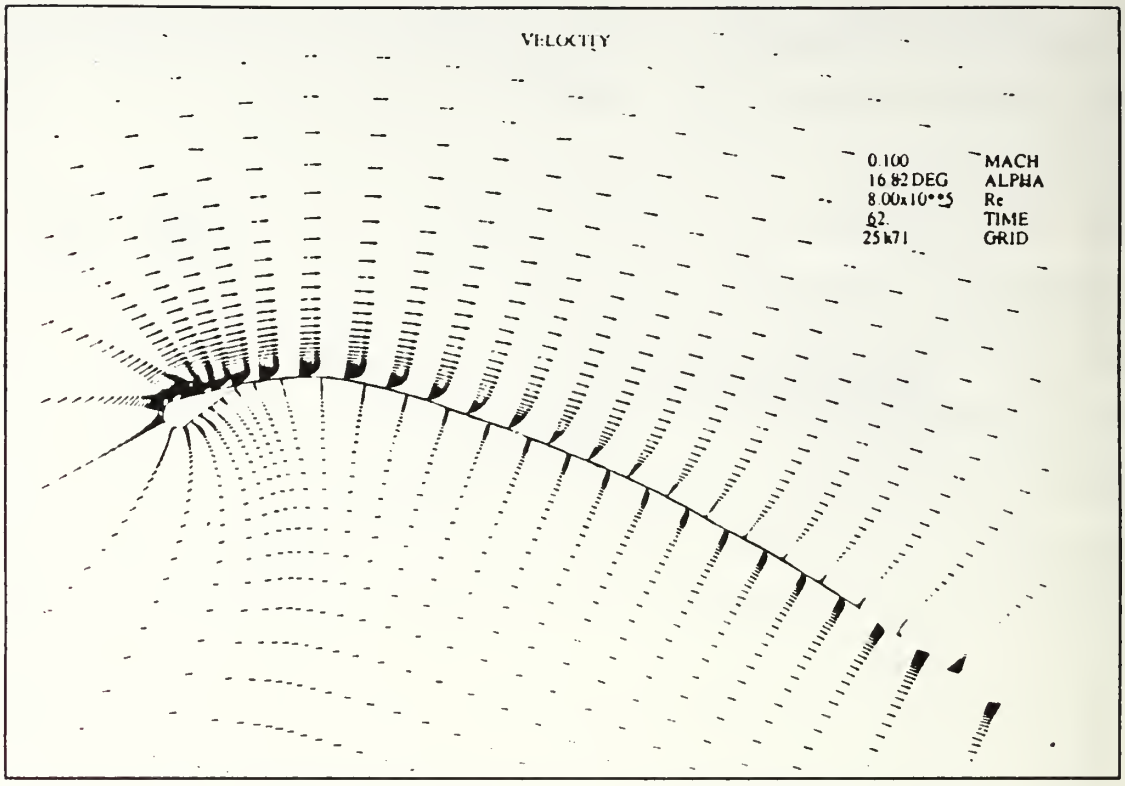

Figure 4.24 Unsteady Motion - 16.82 degrees

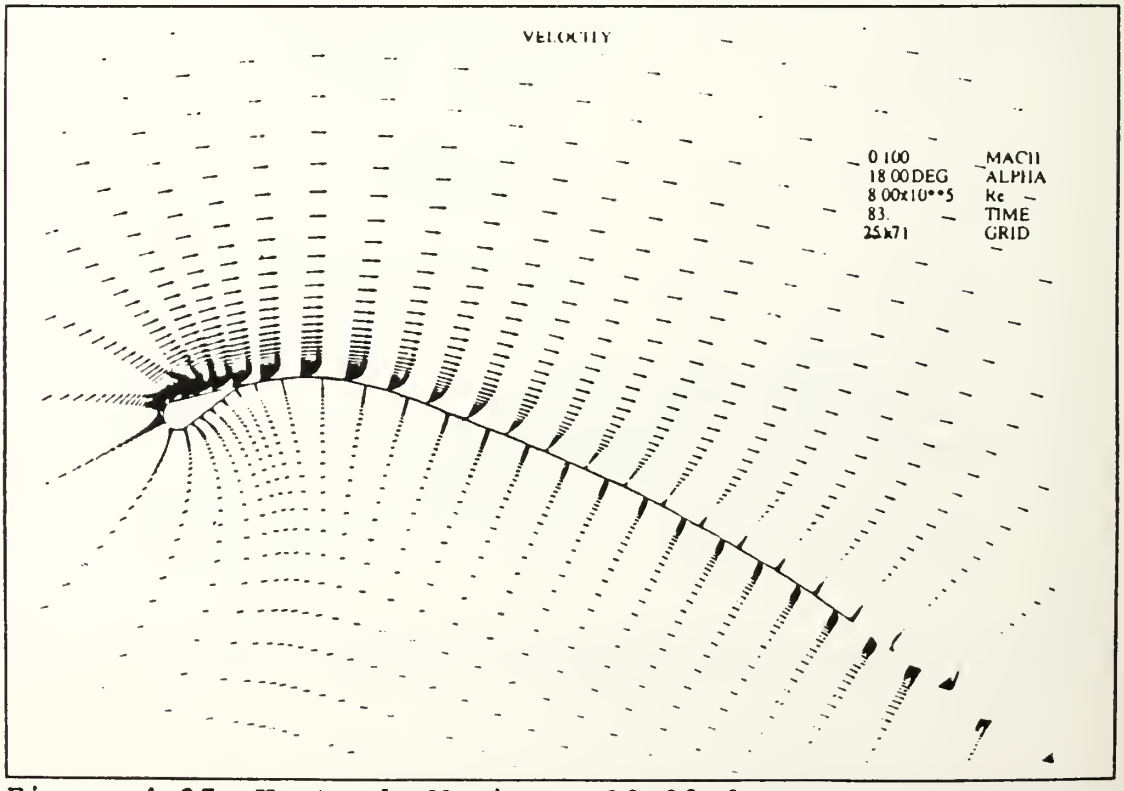

Figure 4.25 Unsteady Motion - 18.00 degrees

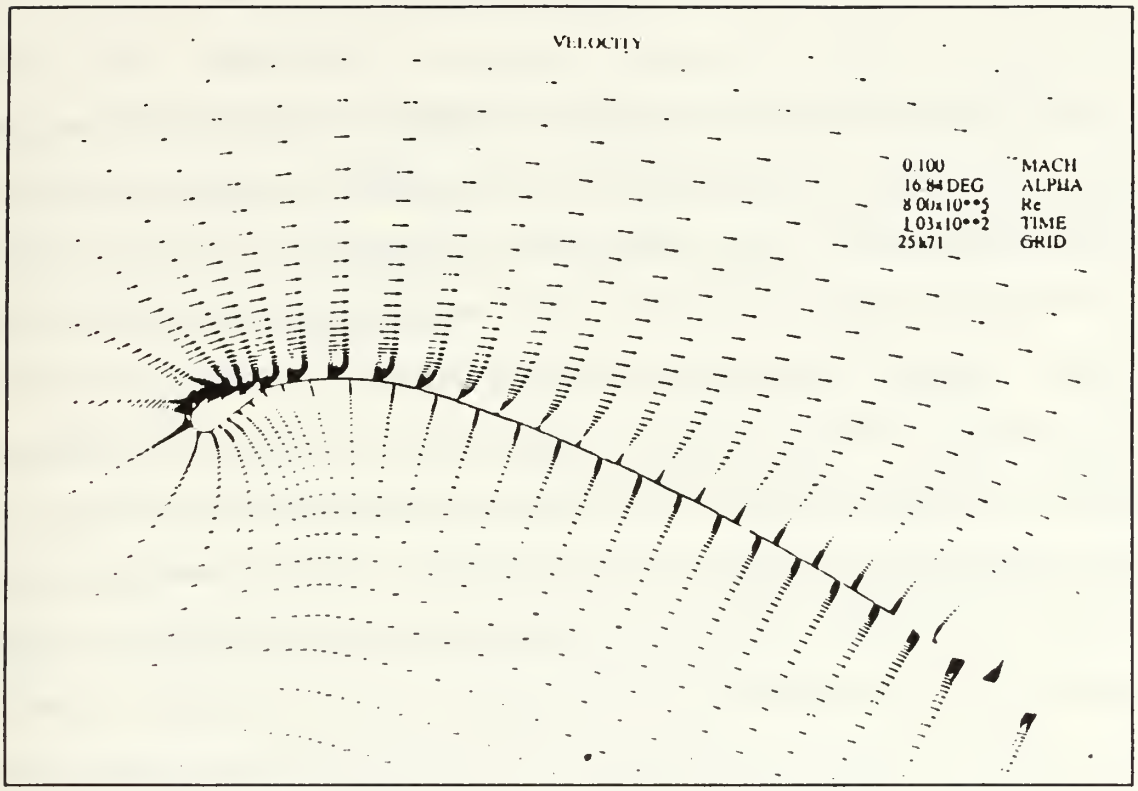

Figure 4.26 Unsteady Motion - 16.82 degrees

V. CONCLUSIONS

In the computational and experimental investigation of the flow field about windsurfing sail sections several important findings were made. The first area of surprise was the extent of flow separation that is present over several areas on the sections. This was evident in both the Navier-Stokes calculations and in the flow visualization experiments. Moreover, the degree of separation was the primary reason for the failure of the two boundary layer methods that were applied to this problem. While the panel method represents the most elementary code used on the problem it compared favorably with the more costly inviscid Euler routine. Since the Euler code is nearly as expensive in computer time as the Navier-Stokes method its use can not be justified. Instead, much useful information can be obtained from the Navier-Stokes solutions.

The Navier-Stokes code, 'ns2.f', while performing well, has been improved upon. Specifically, a variable time stepping routine has been added which offers a reduction in the number of iterations and computer time by over one half. Only one turbulence model, Baldwin-Lomax, was incorporated in the version that was evaluated in the thesis. Several other models have since been added and could be evaluated. Further investigations of the effect of sail pumping used in competitive board sailing would be of high interest to sailors and to aerodynamicists. Unfortunately, a failure of the computer system in the CFD laboratory prevented the modeling of a realistic ramp motion for use in 'pumping' simulations.

The experiments undertaken achieved their primary objective to locate the separation regions. However, the visualization experiments could be greatly improved upon. This could be accomplished with the implementation of the laser sheet technique. The rig and model could also be modified to include the examination of unsteady motion effects.

Finally, it is clear that advanced CFD methods, such as Navier-Stokes solvers, can be used in this field. Sail design is a field that thrives on new technology. The advances in computer technology make it only a matter of time when CFD techniques will migrate to the field of sail design.

LIST OF REFERENCES

1. Anderson, J. D., Fundamentals of Aerodynamics, @d ed., McGraw-Hill, Inc., 1991.

2. Cricelli, A. S., Ekaterinaris, J. A., Platzer, M. F., "Unsteady Airfoil Solutions on Moving Zonal Grids," AIAA-92-0543, Presented at the 30th Aerospace Sciences Meeting & Exhibit, Reno, NV, January 6-9, 1992.

3. Marchai, C. A., Aero-Hydrodynamics of Sailing, Dodd, Mead & Company, 1979.

4. Marchai, C. A., Sailing Theory and Practice, Dodd,Mead & Company, 1982.

5. Merkle, C. L., Computational Fluid Dynamics of Inviscid and High Reynolds Number Flows, Procopy, Inc., 1990.

6. Nowak, L. M., Computational Investigations of a NACA 0012 in Low Reynolds Number Flows, Engineer's Thesis, Naval Postgraduate School, Monterey, CA, September 1992.

7. Smith, R. W., "An Inviscid Analysis of the Flow About Windsurfing Sails," Presented at the 17th Annual AIAA Symposium on Sailing, Stanford, CA, Saturday and Sunday, October 31, November 1, 1987,

8. Sommers, J. D., An Experimental Investigation of Support Strut Interference on a Three-Percent Fighter Model at High Angles of Attack, Master of Science Thesis, Naval Postgraduate School, Monterey, CA, September 1989

APPENDIX A: COMPUTER PROGRAMS

Some of the computer programs that were used during the research are presented in the following section. This listing is by no means a complete listing of the software utilized. Not listed but of significant utility are 'hypgen' and 'plot3d' both of which are well documented.

```
*****  shape.f
* Lt Matthew Avila
* Thesis Advisor: Prof Platzer
* Sail section generation subroutine
* Parabolic/circular arc or Lagrange Interpolation
*     to define camber line
* Wake points added for hypgen use        ( hypgen.dat )
* X-Y data points                         ( shape.out )
*****
      DIMENSION X(0:150),Y(0:150),XNODE(30),YNODE(30)
      DIMENSION xx(300),yy(300),zz(300),Xwake(30),Ywake(30)
      OPEN (101,FILE='shape.out',STATUS='UNKNOWN')
      OPEN (102,FILE='hypgen.dat',FORM='formatted')
      pi=3.14159265
      X(0)=1.0
      Y(0)=0.0
      X(150)=1.0
      Y(150)=0.0

      PRINT *,'This program generates X-Y section coordinates and'
      PRINT *,'Plot3d file for with the HYPGEN grid generation
program.'
      PRINT *,'151 points are created for the X-Y plot and a
211x1x1'
      PRINT *,'grid in plot3d format.'

10    PRINT *,'Enter camber line generation method'
      PRINT *,'       1 = parabola forward section / circular arc
aft'
      PRINT *,'       2 = Lagrange polynomial defined by user'
      READ *,TYPE

      IF (TYPE.EQ.1) THEN
            GOTO 20
         ELSEIF (TYPE.EQ.2) THEN
            GOTO 50
         ELSE
            PRINT *,'You must enter 1 or 2'
            GOTO 10
      ENDIF

* Input Variables for Parabolic-arc method
20    PRINT *,'Enter mast radius (.02 normal)'
      READ *,r
      PRINT *,'Enter Maximum camber'
      READ *,Ymax
      PRINT *,'Enter Maximum camber location'
      READ *,Xmax
      PRINT *,'Enter Luff Pocket Length'
      READ *,Xluff
      PRINT *,'Enter thickness'
      READ *,t
```

```
      t=t/2
      nfwd=INT(Xluff*70)
      naft=70-nfwd
      r1=((1-Xmax)**2+Ymax**2)/2/Ymax

*  Aft sections / Parabolic-Arc
      dxaft=(1-Xluff)/naft
      DO 30 I=1,naft
     Xl=I*dxaft
        IF (Xl.LE.(1-Xmax)) THEN
           Si=ASIN((1-Xmax-Xl)/r1)
           Yl=r1*COS(Si)+Ymax-r1
        ELSE
           Yl=Ymax-Ymax*((Xl+Xmax-1)**2)/(Xmax**2)
        ENDIF
        X(I)=1.0-Xl
        Y(I)=Yl-t
        X(150-I)=1.0-Xl
        Y(150-I)=Yl+t
30    CONTINUE

* Wake section / parabolic-Arc
      Si = ASIN( (1.-Xmax) / (r1-Ymax) )
      Xwake(1)=1+dxaft
      Ywake(1)=-dxaft*TAN(Si)
      DO 40 I=2,30
        dxaft=dxaft*1.2
        Xwake(I)=Xwake(I-1)+dxaft
        Ywake(I)= - ( Xwake(I) -1. )*TAN(Si)
40    CONTINUE
      GOTO 100

* Input Variables for the Lagrange method
50    PRINT *,'Enter number of nodes to describe camber line'
      READ *,nn
      DO 60 I=1,nn
         PRINT *,'Enter (x,y) for node',I
         READ *,XNODE(I),YNODE(I)
60    CONTINUE

      PRINT *,'Enter mast radius (.02 normal)'
      READ *,r
      PRINT *,'Enter Luff Pocket Length'
      READ *,Xluff
      PRINT *,'Enter thickness'
      READ *,t
      t=t/2
      nfwd=INT(Xluff*70)
      naft=70-nfwd

*  Aft sections / Lagrange method
      dxaft=(1-Xluff)/naft
```

```
      DO 70 I=1,naft
     Xl = 1 - I*dxaft
        Yl=0
           DO 80 K=1,nn
              Z = YNODE(K)
              DO 90 L=1,nn
              IF (K.NE.L) Z=Z*(Xl-XNODE(L))/(XNODE(K)-XNODE(L))

90            CONTINUE
              Yl = Yl + Z
80         CONTINUE

        X(I) = Xl
        Y(I) = Yl-t
        X(150-I) = Xl
        Y(150-I) = Yl+t
70    CONTINUE

* Wake section / Lagrange
100   Si = ATAN((Y(1)+Y(149))/2/dxaft)
      Xwake(1)=1+dxaft
      Ywake(1)=-dxaft*TAN(Si)
      DO 110 I=2,30
        dxaft=dxaft*1.2
        Xwake(I)=Xwake(I-1)+dxaft
        Ywake(I)= - ( Xwake(I) -1. )*TAN(Si)
110    CONTINUE

* Lower Luff Section / Common for both methods
      The1=pi/2-ATAN(Y(naft)/(Xluff-r))
      X(70)=r+r*COS(the1)
      Y(70)=-r*SIN(The1)
      dx=X(70)-X(naft)
      slope=(Y(70)-Y(naft))/dx
      dxfwd=dx/nfwd
      DO 120 I=1,(nfwd-1)
        X(I+naft)=Xluff+dxfwd*I
        Y(I+naft)=Y(naft)+(X(I+naft)-X(naft))*slope
120    CONTINUE

* Upper Luff Section / Common both methods
      The2=pi/2-ATAN((Xluff-r)/Y(150-naft))
      X(80)=r-r*SIN(The2)
      Y(80)=r*COS(The2)
      dx=X(150-naft)-X(80)
      slope=(Y(150-naft)-Y(80))/dx
      dxfwd=dx/nfwd
      DO 130 I=1,(nfwd-1)
        X(I+80)=X(80)+dxfwd*I
        Y(I+80)=Y(80)+(X(I+80)-X(80))*slope
130    CONTINUE
```

```
* Leading Edge Section
      Theda=1.50*pi-The1-The2
      dTheda=Theda/10
      DO 140 I=1,9
        X(70+I)=r+r*COS(dTheda*I+The1)
        Y(70+I)=-r*SIN(dTheda*I+The1)
140    CONTINUE


* SHAPE.OUT ROUTINE

      DO 150 I=0,150
         WRITE (101,*)X(I),Y(I)
150   CONTINUE


* HYPGEN ROUTINE

       im = 211
       jm = 1
       km = 1

       j=0
       do 160 i=30,1,-1
       j=j+1
       xx(j)=Xwake(i)
       yy(j)=0.
       zz(j)=Ywake(i)
160    continue

       do 170 i=0,150
       ii = i+31
       xx(ii) = x(i)
       yy(ii) = 0.
       zz(ii) = y(i)
170    continue

       do 180 i=1,30
       xx(i+181)=Xwake(i)
       yy(i+181)=0.
       zz(i+181)=Ywake(i)
180    continue

      rewind 102
      write (102,*) 1
      write (102,*) im,jm,km
      write (102,*) (xx(i), i=1,211),
     >              (yy(i), i=1,211),
     >              (zz(i), i=1,211)
      close (102)

      END
```

***** Shape.out - Primary section - 11.5 % chamber

***** point	X	Y
0	1.000000	0.000000E+00
1	9.817000E-01	3.269569E-03
2	9.634000E-01	8.880347E-03
3	9.451000E-01	1.433349E-02
4	9.268000E-01	1.963011E-02
5	9.085000E-01	2.477126E-02
6	8.902000E-01	2.975801E-02
7	8.719000E-01	3.459128E-02
8	8.536000E-01	3.927206E-02
9	8.353000E-01	4.380124E-02
10	8.170000E-01	4.817970E-02
11	7.987000E-01	5.240830E-02
12	7.804000E-01	5.648780E-02
13	7.621000E-01	6.041901E-02
14	7.438000E-01	6.420265E-02
15	7.255000E-01	6.783941E-02
16	7.072000E-01	7.133000E-02
17	6.889000E-01	7.467502E-02
18	6.706000E-01	7.787510E-02
19	6.523000E-01	8.093083E-02
20	6.340000E-01	8.384275E-02
21	6.157000E-01	8.661140E-02
22	5.974000E-01	8.923726E-02
23	5.791000E-01	9.172080E-02
24	5.608000E-01	9.406247E-02
25	5.425000E-01	9.626268E-02
26	5.242000E-01	9.832182E-02
27	5.059000E-01	1.002402E-01
28	4.876000E-01	1.020183E-01
29	4.693000E-01	1.036563E-01
30	4.510000E-01	1.051545E-01
31	4.327000E-01	1.065132E-01
32	4.144000E-01	1.077326E-01
33	3.961000E-01	1.088129E-01
34	3.778000E-01	1.097544E-01
35	3.595000E-01	1.105571E-01
36	3.412000E-01	1.112212E-01
37	3.229000E-01	1.117469E-01
38	3.046000E-01	1.121341E-01
39	2.863000E-01	1.123831E-01
40	2.680000E-01	1.124938E-01
41	2.497000E-01	1.122266E-01
42	2.314000E-01	1.108858E-01
43	2.131000E-01	1.084272E-01
44	1.948000E-01	1.048508E-01
45	1.765000E-01	1.001566E-01
46	1.582000E-01	9.434451E-02
47	1.399000E-01	8.741464E-02
48	1.216000E-01	7.936696E-02
49	1.033000E-01	7.020146E-02

50	8.499998E-02	5.991813E-02
51	8.242778E-02	5.618700E-02
52	7.985556E-02	5.245582E-02
53	7.728335E-02	4.872465E-02
54	7.471112E-02	4.499348E-02
55	7.213891E-02	4.126231E-02
56	6.956669E-02	3.753114E-02
57	6.699447E-02	3.379996E-02
58	6.442225E-02	3.006879E-02
59	6.185003E-02	2.633762E-02
60	5.927781E-02	2.260645E-02
61	5.670559E-02	1.887528E-02
62	5.413337E-02	1.514410E-02
63	5.156115E-02	1.141293E-02
64	4.898893E-02	7.681764E-03
65	4.641671E-02	3.950591E-03
66	4.384449E-02	2.194186E-04
67	4.127228E-02	-3.511754E-03
68	3.870006E-02	-7.242926E-03
69	3.612784E-02	-1.097409E-02
70	3.355560E-02	-1.470530E-02
71	2.842064E-02	-1.814092E-02
72	2.248211E-02	-1.984538E-02
73	1.630672E-02	-1.965603E-02
74	1.048377E-02	-1.759094E-02
75	5.568937E-03	-1.384718E-02
76	2.031239E-03	-8.782006E-03
77	2.082685E-04	-2.878779E-03
78	2.739891E-04	3.299166E-03
79	2.222129E-03	9.162276E-03
80	5.866778E-03	1.415104E-02
81	9.823438E-03	1.668940E-02
82	1.378010E-02	1.922775E-02
83	1.773676E-02	2.176611E-02
84	2.169342E-02	2.430446E-02
85	2.565008E-02	2.684281E-02
86	2.960674E-02	2.938117E-02
87	3.356340E-02	3.191952E-02
88	3.752005E-02	3.445788E-02
89	4.147672E-02	3.699623E-02
90	4.543338E-02	3.953459E-02
91	4.939003E-02	4.207294E-02
92	5.334669E-02	4.461129E-02
93	5.730335E-02	4.714965E-02
94	6.126001E-02	4.968800E-02
95	6.521668E-02	5.222636E-02
96	6.917334E-02	5.476471E-02
97	7.313000E-02	5.730307E-02
98	7.708665E-02	5.984142E-02
99	8.104331E-02	6.237977E-02
100	8.499998E-02	6.491813E-02
101	1.033000E-01	7.520145E-02

102	1.216000E-01	8.436695E-02
103	1.399000E-01	9.241464E-02
104	1.582000E-01	9.934451E-02
105	1.765000E-01	1.051566E-01
106	1.948000E-01	1.098508E-01
107	2.131000E-01	1.134272E-01
108	2.314000E-01	1.158858E-01
109	2.497000E-01	1.172266E-01
110	2.680000E-01	1.174938E-01
111	2.863000E-01	1.173831E-01
112	3.046000E-01	1.171341E-01
113	3.229000E-01	1.167469E-01
114	3.412000E-01	1.162212E-01
115	3.595000E-01	1.155571E-01
116	3.778000E-01	1.147543E-01
117	3.961000E-01	1.138129E-01
118	4.144000E-01	1.127326E-01
119	4.327000E-01	1.115132E-01
120	4.510000E-01	1.101545E-01
121	4.693000E-01	1.086563E-01
122	4.876000E-01	1.070183E-01
123	5.059000E-01	1.052402E-01
124	5.242000E-01	1.033218E-01
125	5.425000E-01	1.012627E-01
126	5.608000E-01	9.906247E-02
127	5.791000E-01	9.672080E-02
128	5.974000E-01	9.423725E-02
129	6.157000E-01	9.161139E-02
130	6.340000E-01	8.884274E-02
131	6.523000E-01	8.593082E-02
132	6.706000E-01	8.287510E-02
133	6.889000E-01	7.967501E-02
134	7.072000E-01	7.632999E-02
135	7.255000E-01	7.283941E-02
136	7.438000E-01	6.920265E-02
137	7.621000E-01	6.541901E-02
138	7.804000E-01	6.148781E-02
139	7.987000E-01	5.740830E-02
140	8.170000E-01	5.317971E-02
141	8.353000E-01	4.880124E-02
142	8.536000E-01	4.427206E-02
143	8.719000E-01	3.959129E-02
144	8.902000E-01	3.475801E-02
145	9.085000E-01	2.977126E-02
146	9.268000E-01	2.463011E-02
147	9.451000E-01	1.933349E-02
148	9.634000E-01	1.388035E-02
149	9.817000E-01	8.269569E-03
150	1.000000	0.000000E+00

***** Shape.out - 8.5 % chamber section

***** point	X	Y
0	1.000000	0.000000E+00
1	9.830000E-01	2.340039E-03
2	9.660000E-01	7.030208E-03
3	9.490000E-01	1.157152E-02
4	9.320000E-01	1.596496E-02
5	9.150000E-01	2.021145E-02
6	8.980000E-01	2.431186E-02
7	8.810000E-01	2.826707E-02
8	8.640000E-01	3.207787E-02
9	8.470000E-01	3.574507E-02
10	8.300000E-01	3.926940E-02
11	8.130000E-01	4.265158E-02
12	7.960000E-01	4.589228E-02
13	7.790000E-01	4.899215E-02
14	7.620000E-01	5.195180E-02
15	7.450000E-01	5.477183E-02
16	7.280000E-01	5.745278E-02
17	7.110000E-01	5.999517E-02
18	6.940000E-01	6.239951E-02
19	6.770000E-01	6.466625E-02
20	6.600000E-01	6.679583E-02
21	6.430000E-01	6.878867E-02
22	6.260000E-01	7.064513E-02
23	6.090000E-01	7.236557E-02
24	5.920000E-01	7.395033E-02
25	5.750000E-01	7.539970E-02
26	5.580000E-01	7.671394E-02
27	5.410000E-01	7.789332E-02
28	5.240000E-01	7.893805E-02
29	5.070000E-01	7.984833E-02
30	4.900000E-01	8.062432E-02
31	4.730000E-01	8.126617E-02
32	4.560000E-01	8.177400E-02
33	4.390000E-01	8.214792E-02
34	4.220001E-01	8.238797E-02
35	4.050000E-01	8.249421E-02
36	3.880000E-01	8.242350E-02
37	3.710001E-01	8.205322E-02
38	3.540000E-01	8.137588E-02
39	3.370000E-01	8.039147E-02
40	3.200001E-01	7.910001E-02
41	3.030000E-01	7.750148E-02
42	2.860000E-01	7.559588E-02
43	2.690001E-01	7.338323E-02
44	2.520000E-01	7.086351E-02
45	2.350000E-01	6.803672E-02
46	2.180001E-01	6.490289E-02
47	2.010000E-01	6.146197E-02
48	1.840000E-01	5.771400E-02
49	1.670001E-01	5.365898E-02

50	1.500000E-01	4.929688E-02
51	1.438546E-01	4.589699E-02
52	1.377091E-01	4.249712E-02
53	1.315637E-01	3.909725E-02
54	1.254183E-01	3.569737E-02
55	1.192728E-01	3.229750E-02
56	1.131274E-01	2.889762E-02
57	1.069820E-01	2.549775E-02
58	1.008365E-01	2.209787E-02
59	9.469112E-02	1.869801E-02
60	8.854569E-02	1.529813E-02
61	8.240025E-02	1.189826E-02
62	7.625482E-02	8.498384E-03
63	7.010939E-02	5.098510E-03
64	6.396396E-02	1.698636E-03
65	5.781852E-02	-1.701238E-03
66	5.167309E-02	-5.101112E-03
67	4.552766E-02	-8.500986E-03
68	3.938223E-02	-1.190086E-02
69	3.323679E-02	-1.530073E-02
70	2.709139E-02	-1.870059E-02
71	2.103181E-02	-1.997337E-02
72	1.487334E-02	-1.933177E-02
73	9.206233E-03	-1.683730E-02
74	4.573669E-03	-1.272903E-02
75	1.419661E-03	-7.400743E-03
76	4.650643E-05	-1.363119E-03
77	5.858173E-04	4.805154E-03
78	2.985903E-03	1.051287E-02
79	7.016724E-03	1.521297E-02
80	1.229194E-02	1.845497E-02
81	1.917735E-02	2.024706E-02
82	2.606275E-02	2.203916E-02
83	3.294816E-02	2.383126E-02
84	3.983356E-02	2.562335E-02
85	4.671897E-02	2.741545E-02
86	5.360437E-02	2.920754E-02
87	6.048977E-02	3.099964E-02
88	6.737518E-02	3.279173E-02
89	7.426059E-02	3.458383E-02
90	8.114599E-02	3.637592E-02
91	8.803140E-02	3.816802E-02
92	9.491680E-02	3.996012E-02
93	1.018022E-01	4.175221E-02
94	1.086876E-01	4.354431E-02
95	1.155730E-01	4.533640E-02
96	1.224584E-01	4.712850E-02
97	1.293438E-01	4.892059E-02
98	1.362292E-01	5.071269E-02
99	1.431146E-01	5.250479E-02
100	1.500000E-01	5.429688E-02
101	1.670001E-01	5.865898E-02

102	1.840000E-01	6.271400E-02
103	2.010000E-01	6.646197E-02
104	2.180001E-01	6.990288E-02
105	2.350000E-01	7.303672E-02
106	2.520000E-01	7.586350E-02
107	2.690001E-01	7.838322E-02
108	2.860000E-01	8.059587E-02
109	3.030000E-01	8.250147E-02
110	3.200001E-01	8.410000E-02
111	3.370000E-01	8.539147E-02
112	3.540000E-01	8.637588E-02
113	3.710001E-01	8.705322E-02
114	3.880000E-01	8.742350E-02
115	4.050000E-01	8.749421E-02
116	4.220001E-01	8.738796E-02
117	4.390000E-01	8.714791E-02
118	4.560000E-01	8.677400E-02
119	4.730000E-01	8.626617E-02
120	4.900000E-01	8.562431E-02
121	5.070000E-01	8.484832E-02
122	5.240000E-01	8.393805E-02
123	5.410000E-01	8.289331E-02
124	5.580000E-01	8.171394E-02
125	5.750000E-01	8.039969E-02
126	5.920000E-01	7.895032E-02
127	6.090000E-01	7.736557E-02
128	6.260000E-01	7.564513E-02
129	6.430000E-01	7.378867E-02
130	6.600000E-01	7.179583E-02
131	6.770000E-01	6.966624E-02
132	6.940000E-01	6.739951E-02
133	7.110000E-01	6.499517E-02
134	7.280000E-01	6.245278E-02
135	7.450000E-01	5.977183E-02
136	7.620000E-01	5.695180E-02
137	7.790000E-01	5.399215E-02
138	7.960000E-01	5.089228E-02
139	8.130000E-01	4.765158E-02
140	8.300000E-01	4.426941E-02
141	8.470000E-01	4.074508E-02
142	8.640000E-01	3.707788E-02
143	8.810000E-01	3.326707E-02
144	8.980000E-01	2.931186E-02
145	9.150000E-01	2.521145E-02
146	9.320000E-01	2.096496E-02
147	9.490000E-01	1.657152E-02
148	9.660000E-01	1.203021E-02
149	9.830000E-01	7.340039E-03
150	1.000000	0.000000E+00

```
*****  panel.f
* Lt Matthew Avila                Last modified 19 Oct 92
* Thesis Advisor: Prof Platzer
* Panel Method Program
* Airfoil shape input from Plot3d 2 dimensional grid or
*        X - Y data file
*****
      PARAMETER (ID=300,JD=80)
      COMMON /SET1/X(ID),Y(ID),DIST(ID),SINT(ID),COST(ID)
      COMMON /SET2/A(ID,ID),PI,NPANEL,NODES,NTOT
      DIMENSION XG(ID,JD),YG(ID,JD)
      CHARACTER*80 FILEIN
      INTEGER TYPE
1     FORMAT(A)
      PI=3.1415926585

10    PRINT *,'ENTER DATA TYPE'
      PRINT *,'        1 = PLOT3D FILE'
      PRINT *,'        2 = X - Y DATA'
      READ (*,*)TYPE
      IF (TYPE.EQ.1) THEN
            GOTO 20
         ELSEIF (TYPE.EQ.2) THEN
            GOTO 40
         ELSE
            PRINT *,'YOU MUST ENTER 1 OR 2'
            GOTO 10
       ENDIF

* READ  PLOT3D GRID POINTS FOR AIRFOIL
20    PRINT *,'ENTER 2-D GRID FILE NAME'
      READ (*,1)FILEIN
      OPEN (UNIT=201,FILE=FILEIN,STATUS='OLD',FORM='FORMATTED')
      PRINT *,'ENTER I FOR TRAILING EDGE LOWER, UPPER'
      READ *,ITEL,ITEU
      REWIND 201
      READ (201,*)IMAX,JMAX
      PRINT *,IMAX,JMAX
      READ (201,*)((XG(I,J),I=1,IMAX),J=1,JMAX),
     >     ((YG(I,J),I=1,IMAX),J=1,JMAX)

      I = 0
      DO 30 J=ITEL,ITEU
      I = I + 1
         X(I)=XG(J,1)
         Y(I)=YG(J,1)
30    CONTINUE

      NPANEL = ITEU - ITEL
      NODES  = NPANEL + 1
      NTOT   = NODES + 1
      GOTO 60
```

```
* READ X-Y DATA POINTS FROM A FILE
40     PRINT *,'ENTER X-Y FILE FOR AIRFOIL'
       READ (*,1)FILEIN
       OPEN (UNIT=201,FILE=FILEIN,STATUS='OLD',FORM='FORMATTED')
       PRINT *,'ENTER NUMBER OF DATA POINTS'
       READ *,NODES
       NPANEL = NODES - 1
       NTOT   = NODES + 1

       DO 50 I=1,NODES
          READ (201,*)X(I),Y(I)
50     CONTINUE

* ANGLE OF ATTACK FOR COMPUTATION ENTERED
60     PRINT *,'Enter Angle of attack (degrees)'
       READ *,AOA
       SINA=SIN(AOA*PI/180)
       COSA=COS(AOA*PI/180)

* SLOPE AND LENGTH OF PANELS COMPUTED
       DO 70 J=1,NPANEL
          DX=X(J+1)-X(J)
          DY=Y(J+1)-Y(J)
          DIST(J)=SQRT(DX**2+DY**2)
          SINT(J)=DY/DIST(J)
          COST(J)=DX/DIST(J)
70     CONTINUE

* EXECUTE INFLUENCE COEFFICIENT, GAUSS AND VELOCITY SUBROUTINES
       PRINT *,'PANELS COMPUTED'
       CALL COEFF(SINA,COSA)
       PRINT *,'COEFFICIENTS MATRIX COMPUTED'
       CALL GAUSS(SINA)
       PRINT *,'GAUSS  REDUCTION COMPLETE'
       CALL VELOCITY(SINA,COSA)
       PRINT *,'PRESSURE COEFF. COMPUTED (panel.out)'
       END

**********************************************************************
* INFLUENCE COEFFICIENT SUBROUTINE
       SUBROUTINE COEFF(SINA,COSA)
       PARAMETER (ID=300)
       COMMON /SET1/X(ID),Y(ID),DIST(ID),SINT(ID),COST(ID)
       COMMON /SET2/A(ID,ID),PI,NPANEL,NODES,NTOT

       DO 110 K=1,NODES
       A(NODES,K)=0.0
110    CONTINUE

* MIDPOINT NORMAL VELOCITY=0
* I'th PANEL MIDPOINT
       DO 120 I=1,NPANEL
```

```
          XMID=0.5*(X(I)+X(I+1))
          YMID=0.5*(Y(I)+Y(I+1))
          A(I,NODES)=0.0

*         J 'th PANEL
          DO 130 J=1,NPANEL
             DLN  = 0.0
             BETA = PI
*            I AND J THE SAME
             IF (J.EQ.I) GO TO 140
             DX1  = XMID-X(J)
             DX2  = XMID-X(J+1)
             DY1  = YMID-Y(J)
             DY2  = YMID-Y(J+1)
             D1   = SQRT(DX1**2+DY1**2)
             D2   = SQRT(DX2**2+DY2**2)
             DLN  = LOG(D2/D1)
             BETA=ATAN2(DY2*DX1-DX2*DY1,DX2*DX1+DY2*DY1)
140          SINTIJ=SINT(I)*COST(J)-COST(I)*SINT(J)
             COSTIJ=COST(I)*COST(J)+SINT(I)*SINT(J)
             A(I,J)=(BETA*COSTIJ+DLN*SINTIJ)/PI/2
             B=(DLN*COSTIJ-BETA*SINTIJ)/PI/2
             A(I,NODES)=A(I,NODES)+B
*            KUTTA CONDITION APPLIED TO FIRST/LAST PANEL
             IF ((I.GT.1).AND.(I.LT.NPANEL)) GO TO 130
             A(NODES,J)=A(NODES,J)-B
             A(NODES,NODES)=A(NODES,NODES)+A(I,J)
130       CONTINUE
          A(I,NTOT)=SINT(I)*COSA-COST(I)*SINA
120    CONTINUE
       TEMP=-(COST(1)+COST(NPANEL))*COSA-(SINT(1)+SINT(NPANEL))*SINA
       A(NODES,NTOT)=TEMP
       END

*************************************************************************
* GAUSS SUBROUTINE TO SOLVE COEFFICIENT MATRIX
       SUBROUTINE GAUSS(*)
       PARAMETER (ID=300)
       COMMON /SET1/X(ID),Y(ID),DIST(ID),SINT(ID),COST(ID)
       COMMON /SET2/A(ID,ID),PI,NPANEL,NODES,NTOT

* SEARCH FOR THE LARGEST PIVOT
       DO 200 I=2,NTOT
          IM=I-1
          IMAX=IM
          AMAX=ABS(A(IM,IM))
          DO 210  J=I,NODES
          IF (AMAX.GE.ABS(A(J,IM))) GO TO 210
          IMAX=J
          AMAX=ABS(A(J,IM))
210    CONTINUE
```

```
* SWITCH ROWS IF NECESSARY
      IF (IMAX.EQ.IM) GO TO 220
      DO 230 J    =    IM,NTOT
         TEMP     =    A(IM,J)
         A(IM,J)  =    A(IMAX,J)
         A(IMAX,J)=TEMP
230   CONTINUE

* REDUCE BELOW THE PIVOT DIAGONAL
220   DO 250 J=I,NODES
         R     =    A(J,IM)/A(IM,IM)
         DO 240 K=IM,NTOT
            A(J,K)    =   A(J,K)-R*A(IM,K)
240      CONTINUE
250   CONTINUE

* REDUCE ABOVE THE PIVOT DIAGONAL
      DO 260 J=IM-1,1,-1
         R     =   A(J,IM)/A(IM,IM)
         DO 270 K=IM,NTOT
            A(J,K)    =    A(J,K)-R*A(IM,K)
270      CONTINUE
260   CONTINUE
200   CONTINUE

* CHANGE PIVOT VALUES TO 1.0
      DO 280 I=1,NODES
      A(I,NTOT)=A(I,NTOT)/A(I,I)
      A(I,I)=1.0
280   CONTINUE
      END

*************************************************************************
* VELOCITY DISTRIBUTION SUBROUTINE
      SUBROUTINE VELOCITY(SINA,COSA)
      PARAMETER (ID=300)
      COMMON /SET1/X(ID),Y(ID),DIST(ID),SINT(ID),COST(ID)
      COMMON /SET2/A(ID,ID),PI,NPANEL,NODES,NTOT
      DIMENSION CP(ID),Q(ID)
      OPEN (301,FILE='panel.out',STATUS='unknown')
      YMULT=20.0

      DO 310 I=1,NPANEL
310   Q(I)=A(I,NTOT)
      GAMMA=A(NODES,NTOT)

* I'th PANEL MIDPOINT
      DO 330 I=1,NPANEL
         XMID=0.5*(X(I)+X(I+1))
         YMID=0.5*(Y(I)+Y(I+1))
         VTAN=COSA*COST(I)+SINA*SINT(I)
*        J'th PANEL
```

```
          DO 320 J=1,NPANEL
          DLN=0.0
          BETA=PI
          IF (J.EQ.I) GO TO 300
          DX1  = XMID-X(J)
          DX2  = XMID-X(J+1)
          DY1  = YMID-Y(J)
          DY2  = YMID-Y(J+1)
          D1   = SQRT(DX1**2+DY1**2)
          D2   = SQRT(DX2**2+DY2**2)
          DLN  = LOG(D2/D1)
          BETA=ATAN2(DY2*DX1-DX2*DY1,DX2*DX1+DY2*DY1)
300       SINTIJ=SINT(I)*COST(J)-COST(I)*SINT(J)
          COSTIJ=COST(I)*COST(J)+SINT(I)*SINT(J)
          AA=(BETA*COSTIJ+DLN*SINTIJ)/PI/2
          B=(DLN*COSTIJ-BETA*SINTIJ)/PI/2
          VTAN=VTAN-B*Q(J)+GAMMA*AA
320       CONTINUE
          CP(I)=1.0-VTAN**2
          WRITE (301,*)XMID,CP(I)
330    CONTINUE
       END
```

```
******  rotate.f
* Lt Matthew Avila
* Thesis Advisor: Prof Platzer
* Plot3d grid Rotation Program
*****
      parameter (id=300,kd=80)
      dimension X(id,kd),Z(id,kd)
      character*15 filein,fileout

* Read in original grid
      print *,'Enter plot3d grid file'
10    format(A)
      read (*,10)filein
      open (20,file=filein,form='formatted')
      rewind 20
      read (20,*) imax,kmax
      read (20,*) ((X(i,k),i=1,imax),k=1,kmax),
     >            ((Z(i,k),i=1,imax),k=1,kmax)

* Rotate the grid points
      print *,'Enter the angle to rotate the grid by'
      read (*,*)theta
      theta=theta*3.1415/180
      cost=cos(theta)
      sint=-sin(theta)
      do 30 i=1,imax
      do 30 k=1,kmax
         xold=X(i,k)
         zold=Z(i,k)
         X(i,k)=xold*cost - zold*sint
         Z(i,k)=zold*cost + xold*sint
30    continue

* Write output file
      print *,'Enter filename for rotated grid'
      read (*,10)fileout
      open (40,file=fileout,form='formatted')
      rewind 40
      write (40,*) imax,kmax
      write (40,*) (( X(i,k), i=1,imax), k=1,kmax),
     >          (( Z(i,k), i=1,imax), k=1,kmax)

      stop
      end
```

```
***** ns2.in - input file for ns2.f

  MACH,   ALFA0,   ALFA1,   ALFARE,   REDFRE, REYNOLDS
  0.10,   14.00,     4.0,      0.0,     0.19,     0.80
  ED2X,    ED2Y,    ED4X,     ED4Y,       ED
  0.00,    0.00,   0.030,    0.030,      2.0
    DT,    COUR,   NITER,   NEWTIT
0.0002,   2100.,    2160,        1
 RSTRT,   OSCIL,    RAMP,     NPER    TSHIFT
  true,    true,   false,     1440,     -0.5
TIMEAC,  IMPLBC,   EXPLBC   CIRCOR
     1,   false,    true,    false
  VISC,    BLTM,    JKTM,    RNGTM
  true,    true,   false,    false
  ITEL,    ITEU
    31,     221
UNSTST,  NFRAME
  true,       8,

**********************************************************************
************

Mach      :   Free stream Mach number
Alfa0     :   Agle of attack, also mean angel of attack for unsteady
Alfa1     :   Amplitude of Oscillatory motion
Redfre    :   Reduced frequency k = omege * c / 2U
Reynolds  :   Reynolds number Re = cU/n

ED2x      :   X-direction 2nd order explicit smoothing ( e2x = 0.00
subsonic,
                                                  0.25 < e2x < 0.50
transonic )
ED2z      :   Z-direction 2nd order explicit smoothing ( e2z = 0.00
subsonic,
                                                  0.10 < e2z < 0.20
transonic )
ED4x      :   X-direction 4nd order explicit smoothing ( e4x = 0.03
subsonic,
                                                       e4x = 0.05
transonic )
ED4z      :   Z-direction 4nd order explicit smoothing ( e4z = 0.03
subsonic,
                                                       e4z = 0.05
transonic )
ED        :   Scaling of Implicit smoothing
ISPEC     :   Spectral radious parameter

Dt        :   Time step
Cour      :   Courant Number Cu = dt * L_max
Niter     :   Number of Iteration in this run
Newtit    :   Newton subiteration within each timestep
```

```
RSTRT     :   Restart
OSCIL     :   Oscillatory motion A(t) = A0 + A1 * sin ( k * M * t )
RAMP      :   Ramp motion
NPER      :    Number of time steps in one period of oscillation,
dt=T/Nper
TSHIFT    :   Time shift in radiats to start oscilation for any a(t)

TIMEAC    :    Time accureat Tacc=1 and for Jacobian Scaled Dt,
Tacc=0
IMPLBC    :   Implicit wall bc Treatment
EXPLBC    :   Explicit wall bc Treatment

VISC      :    Viscid or inviscid Boundary Cconditions (if false
inviscid)
TURBL     :   Boldwin-Lomax eddy viscosity (if false laminar only)
JKTM      :   Johnson-King  eddy viscosity (not available)
RNGTM     :   RNG           eddy viscosity (not available)

ITEL, ITEU : Lower and Upper trailing edge I locations

UNSTST (Set true for use with unsteady motion starting from an
steady
        state. This will initialize time = 0 for the unsteady
motion
        that starts from a steady state restart.
NFRAME      :     Number of solutions saved for one cycle of
oscillation.
             Saved starting at unit 41.

Read grid from unit fort.11 and the flow from unit fort.31
```

INITIAL DISTRIBUTION LIST

1.	Defense Technical Information Center Cameron Station Alexandra, Virginia 22304-6145	2
2.	Library, Code 0142 Naval Postgraduate School Monterey, California 93943-5000	2
3.	Dr. M. F. Platzer Department of Aeronautics and Astronautics Code AA/Pl Naval Postgraduate School Monterey, California 93943-5000	7
4.	Chairman Department of Aeronautics and Astronautics Naval Postgraduate School Monterey, California 93943-5000	1
5.	LT M. R. Avila, USN P.O. Box 193 Dowell, Maryland 20629	2
6.	Mr. Trevor Bayless Waddell Sails Inc. 429 Ingalls Street Santa, Cruz, California 95060	1

AMERICAN BINDERY
10
9-93

3 2768 00035903 8